Microwave-assisted hydrothermal synthesis and energy storage application of nickel-aluminum layered double hydroxide-graphene foam nanocomposites

by

Fatemeh Taghizadeh

A thesis submitted in partial fulfillment of the requirements for the degree

Master of Science

Faculty of Natural and Agricultural Sciences

University of Pretoria

Hatfield Pretoria

October 2015

Supervisor/Promoter**: Prof. N. I. Manyala**

Co-supervisor**: Dr. J. K. Dangbegnon**

Declaration

I, Fatemeh Taghizadeh hereby declare that the matter embodied in this thesis entitled "*Microwave-assisted hydrothermal synthesis and energy storage application of nickel-aluminum layered double hydroxide-graphene foam nanocomposites*" is the result of investigations carried out by me under the supervision of Prof. N. Manyala, and co-supervision of Dr. J. Dangbegnon, in the Physics department at the University of Pretoria South Africa and that it has not been submitted by me elsewhere for the award of any degree or diploma. In keeping with the general practice in reporting scientific observations, due acknowledgement has been made whenever the work described is based on the findings of other investigators.

Signature _____ Date_____

Dedication

This desertion is dedicated to my beloved parents who taught me to trust God, for their prayers, supporting and encouraging me to believe in myself and making me who I am.

Acknowledgment

All praises is due to the almighty God, the Lord of the worlds, it is He alone that I worship and it is from Him that I seek help. He is the Creator of all, the Guider of hearts and Master of the day of Judgment. I would not be here today without his blessing, favors, sustenance and grace. Thank you Lord.

I would like to take this opportunity to express my sincere gratitude towards my supervisor Prof. N. Manyala for his support, encouragement, constructive criticism, valuable suggestions and his fatherly guidance. I would also like to express my deepest gratitude to my co-supervisor, Dr. Julien K. Dangbegnon, for his invaluable inputs and for helping me with carrying out my laboratory work, as well as for his patience in meticulously analyzing results and working closely with me like an elder brother throughout my Master's Project. Only God can repay them both for all the kindness they have shown towards me.

I would like to give unending appreciation to my father and my mother for their prayers, support, love and encouragement which kept me standing strong throughout all the struggles and frustrations. Also, to my lovely sister, Sepideh, who constantly encouraged and supported me during my work. May God keep you all in good Health.

My special gratitude goes to my longtime friends and brothers, Mr. Farshad Barzegar and Mr. Kian Ostvar for their encouragement, help and also to my great colleagues and friends, Dr. Abdulhakeem Bello and Dr. Damilola Yusuf Momodu for giving me unending assistance and guidance in both the experimental and theoretical parts of my research.

I would also like to express my gratitude to the rest of my research group members, Ms. Masikhwa T. M., Mr. Madito J M., Dr. Fabiane M., Mr. Khaleed A., Ms. Ugbo F. and Mr. Olaniyan O. for their ever-reliable support and assistance they rendered. They will forever remain in my memory.

I would also like to appreciate our generous head of department Prof. C.C Theron for giving me some part-time work in the department in order to enable me to supplement my finances.

I am also thankful to all the great friends I made here at the physics Department, fellow students, staff and professors who put up with me throughout my stay to name a few, my deepest appreciations goes to Ms. A. Singh, Ms. Sh. Vatannia, Mr. M. Moghimi., Ms. H Montaseri, Mrs Isbe van Der Westhuizen and Mrs. Suzette Seymore for their unending support and encouragement during my work.

I am also thankful to Antoinette and Andre at the Microscopy department for their assistance with acquiring SEM images and their analysis and also Dr. Linda Prinsloo for all her assistance with RAMAN measurements.

Once again I say thanks to all the people who have helped me directly or indirectly

Table of Contents

List of figures

List of equations

$$C = \frac{A\varepsilon}{4\pi d} \quad (1)$$

$$\frac{1}{C_T} = \frac{1}{C_p} + \frac{1}{C_n} \quad (2)$$

$$E = \frac{1}{2} CV^2 = \frac{QV}{2} \quad (3)$$

$$P = \frac{1}{4R_s} V^2 \quad (4)$$

$$C_s = \frac{C_i}{m} \quad (5)$$

$$n\lambda = 2d \sin\theta \quad (6)$$

$$Ni(OH)_2 + OH^- \rightarrow NiOOH + H_2O + e^- \quad (7)$$

$$C_s \left(\frac{F}{g}\right) = \frac{\bar{A}}{\upsilon m \Delta V} \quad (8)$$

$$C_{sp} = \frac{It}{m\Delta V} \quad (9)$$

List of Tables

List of Abbreviations and Symbols

Å	Angstrom
Ag/AgCl	Silver – Silver Chloride
BET	Brunauer-Emmett-Teller
BJH	Barrett-Joyner-Halenda
BSE	Back scattered electron
CE	Counter electrode
CD	Galvanostatic charge discharge
CP	Galvanostatic charge discharge
CRT	Cathode ray tube
CV	Cyclic voltammetry
CVD	Chemical vapor deposition
EC_s	Electrochemical capacitors
EDLC	Electrical double-layer capacitor
EES	Electrochemical energy storage
EIS	Electrochemical impedance spectroscopy
ESD	Electrical sequential deposition
E_{OC}	Open circuit potential

FE-SEM	Field emission scanning electron microscopy
FS	Faradic supercapacitor
FTIR	Fourier transform infrared resonance
KOH	Potassium hydroxide
LDH	Layered double hydroxide
LDO_S	Layered double oxides
M^{2+}	Divalent cation material
M^{3+}	Trivalent cation material
M-O	Metal-Oxygen
M-OH	Metal-Hydroxyl
$MWCNT_S$	Multi walled carbon nanotubes
MWI	Microwave irradiation
NMP	N-Metyl-2-Pyrolidone
NO_3^{2-}	Nitrate
OH^-	Hydroxide
PVDF	Polyvinylidene Fluoride
RE	Reference electron
SE^-	Secondary electron

SEM	Scanning electron microscopy
$SWCNT_S$	Single walled carbon nanotubes
WE	Working electrode
XRD	X-ray diffraction
$Z^{'}$	Real impedance
$Z^{''}$	Imaginary impedance
ΔE	Potential differences
ΔV	Voltage range
λ	lambda unit of wavelength

Abstract

The graphene foam (GF) was synthesized by chemical vapor deposition (CVD) and different mass of GF were added to the LDH. The morphological, structural and compositional properties of LDH and LDH/GF composites were investigated by scanning electron microscopy (SEM), X-ray diffraction (XRD), Raman spectroscopy, Fourier transform infrared (FTIR) spectroscopy and Brunauer - Emmett – Teller (BET). The results show the presence of interlaced sheets of LDH/GF composites. The electrochemical properties of the synthesized composite electrode system (with Ag/AgCl as reference electrode) displayed excellent electrochemical performance. All results clearly show and demonstrated excellent potential of graphene based composites electrode materials for energy storage applications.

Chapter 1

1 INTRODUCTION

With the rapid reduction and high consumption of fossil fuels and other natural resources, there is a higher demand for the development and investigation of alternative energy sources (like renewable energy) and clean energy conversion/storage technology that can meet the present energy and power consumption requirements. Presently, conventional energy storage devices like batteries characterized with high energy density but relatively low power output and conventional capacitors with high power densities but low energy output are not capable of meeting these skyrocketing energy demands of future systems [2]. In order to make effective use of new alternative energy technologies, it is important to develop high-performance, low-cost and environmental-friendly energy conversion and storage technology.

Supercapacitors (SCs) also known as electrochemical capacitors (ECs) or ultracapacitors (UCs) are promising alternative energy storage systems due to their relatively fast energy storage and release, high power density and long cycling stability as compared to batteries [3]. SCs have been regarded as the suitable solution for energy storage applications [4–6]. SCs are mostly studied owing to their high charge capacitance and relatively long cycle life. Extensive research has been done on various materials with large and open structures for applications in supercapacitors. However, when it comes to high performance, it has been shown that LDH composites containing electroactive species exhibit very large pseudocapacitive properties [7].

Supercapacitors (SCs) can be divided into two types based on their charge storage mechanisms:

(1) Electrical double-layer supercapacitors (EDLs) where the electrical charge is stored at the interface between the electrode and the electrolyte, and usually is made of carbon-based materials [8,9].

(2) Pseudocapacitors where capacitance arises from reversible faradic reactions that take place at the interface of electrode/electrolyte, and mainly made of transitional metal oxide, conductive polymer and LDH [9].

EDLs have high power density and long cycle life, but suffer from their limited specific capacitance and a low electrochemical energy density. Two ways are in general used to increase the EC energy density:

(i) Hybridize the electrode materials by adding electrochemically active materials (pseudocapacitors or faradaic-like materials) to a carbon based EC electrode layer.

(ii) Completely replace the carbon materials with electrochemically active materials [6].

Pseudocapacitive materials possess relatively high capacitance and fast redox kinetics but lack the mechanical stability and cycle life needed for practical applications. Therefore in order to make fundamental advances in energy conversion and storage, it is important to create and investigate new composite materials. Such composites should be highly capacitive but also mechanically stable to allow designing of better supercapacitors with high specific capacitance, high energy density and long-lasting cycle lives [10].

It is well known that materials with large surface areas and highly ordered structure have better capacitive properties and as a result are expected to exhibit superior performance when applied as electrodes in supercapacitors [10]. Therefore, to achieve the goal of designing highly

capacitive materials, the following factors should be taken into account. Firstly, large specific surface area electroactive materials that can accommodate ions from the electrolyte for fast faradic redox process. Secondly, optimized mass transfer rate of electrolytes, required for fast redox reactions. This can be addressed by providing a suitable mesoporous structure (2-5 nm) and also engineering electroactive materials with multiple oxidation states.

Layered Double Hydroxides (LDHs) as defined by Malak-Polaczyk *et al.* [11], are class of ionic lamellar composites comprised of positively charged host sheets with two types of metallic cations and hydrated anions situated in the interlayer gallery for charge equilibrium. The charge of the sheet arises from the changeover of a part of the divalent metal ions to trivalent ones. Metal ions are octahedrally arranged via six oxygen atoms belonging to six -OH collections. Each -OH collection is communal by three octahedral cations. The general formula for LDH can be written as follows [11]:

$$[M^{2+}_{1-x}\, M^{3+}_{x}\, (OH)_2]^{X+} (A^{n-}_{x/n}).mH_2O \qquad (1)$$

Where M^{2+} represents divalent cation (Mg^{2+}, Fe^{2+}, Co^{2+}, etc.), M^{3+} represent trivalent cation (Al^{3+}, Fe^{3+}, Cr^{3+}, etc.), A^{n-} indicates interlayer anion, x is molar ratio of $M^{3+}/(M^{2+} + M^{3+})$ and m denotes the number of mole of water molecules.

The layers of octahedral brucite-like structure can be delaminated into single layers with 2D anisotropy and positive charge. Depending on the application, various solution-based methods such as flocculation [12], electrical sequential deposition (ESD) [13] and Langmuir-Blodgett [14] method can be used to assemble these inorganic nanosheets into nanocomposites or nanofilm structures. These methods are applied in the synthesis of CoAl LDH, which is the

most-used LDH composite due to its relatively simple synthesis and delamination processes. These methods have also been used for synthesis of composites such as LDH/graphene which have gained popularity in recent years [13]. Most of the Ni-based LDH composite synthesis processes are restricted to an in-situ growth/crystallization on graphene or graphene oxide substrate which could result in highly stacked, large LDH crystals which limits contact between the host layers of LDH and graphene [13]. LDH composites such as Ni-Al, Mg-Al and Ni-Fe LDH in the form of delaminated nanosheets are potentially useful for energy storage application because of their highly electrochemically active surfaces [15].

A group of material that could match the above criteria are graphene-based composites, owing to the unique properties of graphene such as its large surface area (2630 m^2 g^{-1}) [16], high electrical conductivity (~2×10^3 S m^{-1}) [17], adequate mechanical flexibility, high thermal and chemical stability, etc. [16,18]. Graphene can greatly enhance the electrochemical properties of a composite. It consists of sp^2 carbon atoms tightly packed into a honeycomb lattice and, has proved to be an ideal substrate to grow and anchor nanoparticles. LDHs compounds in their pristine form possess low electrical conductivity and have the tendency to stack together in the solid state, therefore are not suitable for specific applications such as in supercapacitors [19]. However LDH incorporated in carbon nanomaterials has an improved electron transport rate, high stability, and large electrolyte contact area, all of which are beneficial for the basic and practical applications of the composites [19]. Layered double hydroxide (LDH)-based materials have been extensively applied in energy storage devices (batteries, supercapacitors and fuel cells) due to their unique properties which includes high surface area, electrical conductivity, chemical stability and low cost [20–23]. LDH/graphene foam composites have been intensively

investigated as promising capacitive materials due to their high redox activity, low cost and the environmentally friendliness of the raw materials used for the synthesis of LDHs [10]

Conventionally, LDH/graphene foam composites are synthesized using the hydrothermal method commonly used to prepare transition metal oxides, ternary systems and inorganic-organic hybrid materials. Hydrothermally synthesized LDHs are generally prepared by mixing the metal salts in water and subsequently adding urea which will favor the hydrolysis. The growth time is over 20 h at a minimum temperature of 120°C [24,25]. This technique provides an efficient way of controlling particle size distribution and macroscopic morphology of nanostructured materials.

For production of metal oxide, bimetallic, semiconductors and metals nanomaterials with controllable size, microwave irradiation (MWI) is an excellent technique [26]. The issue of heating inhomogeneity and relaxed reaction observed in other synthesis techniques such as the normal hydrothermal technique can be eliminated by microwave dielectric heating. Microwave synthesis can be easily scaled-up without suffering from thermal gradient effect. The reason for rapid internal temperature increase is mainly due to the dielectric heating offering important development in the transfer of energy straight to the reactant. This homogenous heating of the core of the nuclei is responsible for the short time of the process with high throughput. It is a clean and easy process, and with modern microwave technology, synthesis procedure is faster and the optimization is easy due to time and temperature programming [27–29].

Microwave energy has been used in many chemical reactions and is prone to change kinetics and selectivity [27]. Energy of microwave is more effective in selective heating in several procedures. A review by Stuegra and Guillard [30] summarizes the microwave process and comes to the conclusion that this technique has only thermal effects.

In this thesis, NiAl LDH/graphene foam (GF) composites were synthesized by microwave irradiation and analyzed by different characterization techniques. Initially, the graphene was prepared by chemical vapor deposition (CVD) and dispersed in an aqueous medium for the microwave synthesis to obtain the composite material for application in supercapacitors.

1.1 Aim and Objectives

A strong motivation for studying pseudocapacitive materials is that it could lead to advancement in high power energy storage devices having high energy densities. The aim of this work is to optimize the reaction time during the synthesis of nickel-aluminum layered double hydroxide NiAl LDH and NiAl LDH/graphene foam (GF) composites by microwave-assisted hydrothermal technique for enhanced electrochemical performance.

The steps taken in this regard are as follows:

I. Synthesis of high quality of graphene foam (GF) samples by chemical vapor deposition on nickel foam substrate.
II. Synthesis of LDH by microwave irradiation technique in different time with different concentration of metal hydroxide.
III. Synthesis of LDH/GF composites by microwave irradiation technique, with different concentration of graphene foam.
IV. Using microwave irradiation method for fabrication of metal hydroxide and metal hydroxide-graphene foam to reduce the time and energy.
V. Investigate the energy storage of LDH and LDH/graphene foam composites
VI. Measurement of the morphological, structural and pore size distribution of the LDH and LDH/GF composites with different techniques such as scanning electron microscopy

(SEM), x-ray diffraction method (XRD), Fourier transform infrared (FTIR) spectroscopy, Raman spectroscopy and Barrett-Joyner-Halenda (BJH) technique.

VII. Measurement of the electrochemical performance and characteristic of the LDH and LDH/GF composites electrodes by understanding the principles of its charge storage mechanisms.

1.2 Outline of thesis

This work is divided into five (5) chapters: Chapter 1 and 2 present an introduction and literature review on synthesis techniques of NiAl LDH/GF composites and their application as supercapacitors, respectively. Chapter 3 presents the experimental techniques while chapter 4 will deal with results and discussion. A summarized conclusion from the discussed results will be presented in chapter 5, with possible suggestions for future work to be performed on the composite material.

Chapter 2

2 LITERATURE REVIEW

2.1 SUPERCAPACITORS AND PSEUDOCAPACITORS

Batteries and supercapacitors are two kinds of electrochemical energy storage (EES) systems that are extensively used for powering the now-ubiquitous portable electronics and for the electrification of the transport subdivision in our society. The emerging necessity to renovate the power network in several industrialized countries together with the predictable rise in global energy needs in the future years, have brought in additional utilization for EES which could be paired with renewable energy sources such as solar and wind. Although EES have a wide range of potential application, they face some challenges that are essentially related to finding materials that are both capable of storing and delivering substantial amount of energy in very short time Ideally, materials used for EES should be abundant, non-toxic, cost effective and environmental friendly [31].

Owing to the high energy density of batteries but low power density, they can power devices throughout the day. However, charging a battery is time consuming since it can take hours to be fully charged. For fast power delivery and recharging requirements, supercapacitors are preferred used. In other words, supercapacitors have high power density compared to batteries. Both batteries and supercapacitors depend on the electrochemical processes, although distinct electrochemical mechanisms define their power and energy densities. Furthermore, these differences also give rise to different charge storage properties [32]. In lithium-ion batteries, for

example, the insertion of Li^+ that allows redox reactions in the majority of electrode materials is diffusion controlled and can be relatively slow. On the other hand, electrical double-layer capacitor (EDLC) or supercapacitors store charge by adsorption of electrolyte ions on the surface of electrode materials. In EDLC, redox reactions are not necessary, thus the response to changes in potential without diffusion limitations is fast and leads to high power. However, since the charges are confined to the surface of the electrode only, the energy density is less than that of batteries. Moreover, due to no or scarce chemical reactions, electrochemical capacitor (EC) are predicted to have a longer cycle life than batteries [5].

In pseudocapacitor or redox capacitor, reversible redox reaction takes place at or close to the surface of an suitable electrode material, leading to extremely high charge storage and energy density [32]. Three kinds of faradaic procedures happen at pseudocapacitor electrode: reversible adsorption, redox reactions of transition metal oxides (for example RuO_2) and reversible electrochemical doping/de-doping in conductive polymer based electrodes. Faradaic electrochemical processes also increase the specific capacitance and extend the working voltage. Conway *et al.* [33] showed that since the electrochemical procedures happen both on the surface and in the bulk, near the surface of the solid electrode, a Faradaic supercapacitor (FS) displays larger capacitance values and energy density than an electrical double-layer supercapacitor (EDLCs), and the capacitance can be 10-100 times greater than electrostatic capacitance [6].

In summary, EC can be classified in two main groups due to the charge storage mechanism:

(1) EDLCs where the materials used are carbon-based such as activated carbon, carbon nanotubes, graphene and etc [13,34].
(2) Pseudocapacitor (redox electrochemical capacitors), where the electrode materials can be transition metal oxide/hydroxides and conductive polymer [2,34,35].

Electrochemical capacitors (ECs) have started attracting attention from 1990 when it was found that they can boost batteries or fuel cells in a hybrid electric car, providing the necessary power during the acceleration stage. It could also store energy previously lost during the braking stage [36]. Recently, ECs were used as complement to batteries or fuel cell in their energy storage functions as back-up power supplies [6].

The recent achievement of ECs is in large part due to the use of transition metal oxides/hydroxides into one or both electrodes. The main difference between batteries and pseudocapacitive materials is that the charging/discharging times of pseudocapacitive materials happen in the order of seconds and minutes. Figure 2.1, displays the specific energy vs. charging time plot for an EDLC and a high-rate lithium ion battery. This plot clearly proves that a lithium ion battery optimized for high-power shows constant energy density for discharge time greater than 10 minutes [31].

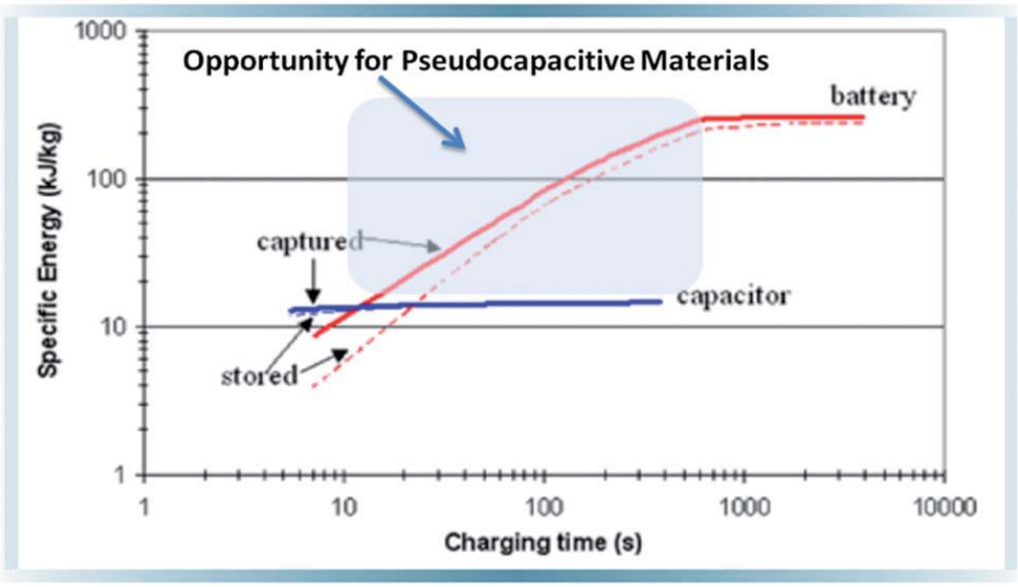

Figure 2.1: Energy vs. charging time for an EDLC and a lithium-ion battery. The region between 10 s and 10 minutes represents the time domain where high-rate pseudocapacitive materials could offer higher energy and power densities than lithium-ion batteries and EDLCs [31].

At shorter timescales, resistive losses within the battery are responsible for the drop in energy. This becomes a serious safety issue at very small charging time or high charging rate where these resistive losses generate heat. On the other hand, current commercially available EDLCs display constant energy density for the whole periods but their overall stored energy is low. In between the timescales where EDLCs and lithium-ion batteries have their peak performance, there exists a time domain (~10 s to 10 minutes) that seems well-suited for the pseudocapacitive materials [31].

2.1.1 Fundamentals, voltage, power and energy of electrochemical capacitor (EC)

An Electrochemical Capacitor (EC) involves two electrodes (which are one of its most important parts), an electrolyte, and a separator that electrically insulates the electrodes. From Fig. 2, it can be seen that charge can be stored and separated at the interface between the conductive solid particles (for example metal oxide particle or carbon particle) and the electrolyte. This interface can be considered as a capacitor with a double-layer capacitance, expressed as follows:

$$C = \frac{A\varepsilon}{4\pi d} \quad (1)$$

Where A is the area of the electrode surface, ε is the electrolyte dielectric constant and d is the effective thickness of the electrical double layer.

The whole cell can therefore be considered as two capacitors in series, with C_p and C_n capacitances for the positive and negative electrode, respectively. If C_T is total capacitance of the whole cell, it can be expressed as follows:

$$\frac{1}{C_T} = \frac{1}{C_p} + \frac{1}{C_n} \quad (2)$$

The theoretical energy (E) and power (P) densities can be expressed by eqn (3) and eqn (4):

$$E = \frac{1}{2} CV^2 = \frac{QV}{2} \quad (3)$$

$$P = \frac{1}{4R_s} V^2 \quad (4)$$

Where Q is the total charges stored, R_s is the corresponding inner resistance of the ES. V is the operating voltage and C the capacitance of the cell. Therefore, the determining variables influencing the device performance are V, C and R_s; in other words, increasing values of V and

C with simultaneous decreasing value of R_s will significantly increase both the energy and power densities [6].

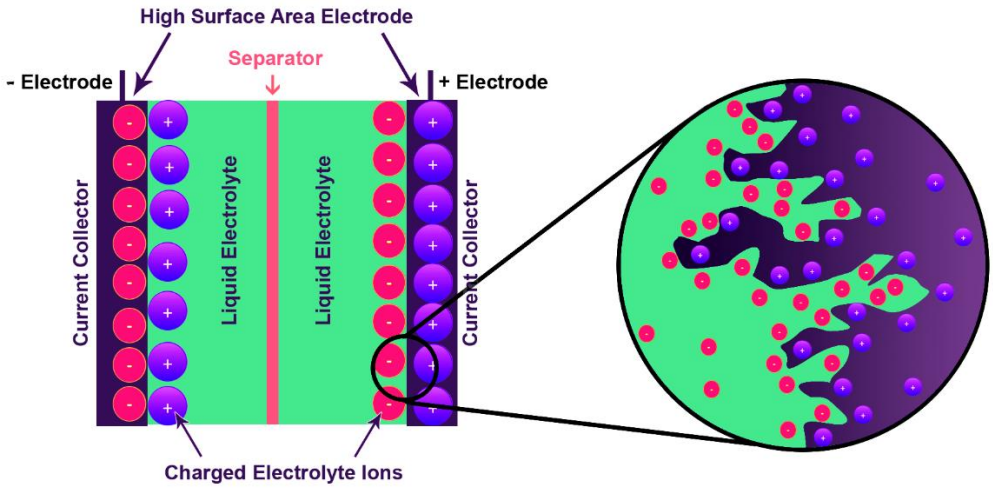

Figure 2.2: Principles of a single-cell double-layer capacitor and illustration of the potential drop at the electrode/electrolyte interface

The specific capacitance with a unit of Faraday per gram (F g^{-1}) is the intrinsic capacitance of the material. Also, higher specific capacitance of a material does not guarantee that this material will be better for EC since its capacitance is strongly dependent on the electrode layering structure, the electron and ion transfers within the layers [6]. The specific gravimetric capacitance is expressed as follows:

$$C_s = \frac{C_i}{m} \qquad (5)$$

where C_i is either the capacitance of the positive or negative electrode and m is the mass in grams of the corresponding electrode.

2.1.2 Electrolytes

The electrolyte is another important component of the EC. The electrolyte can be divided into 3 different types:

(i) Organic electrolyte

(ii) Ionic liquids (ILs) and

(iii) Aqueous electrolyte.

In this dissertation, only an aqueous electrolyte will be used due to its cost effectiveness and environment friendly nature. These electrolytes can be divided into three groups depending on their pH namely:

- Base electrolyte such as KOH, for pH > 7
- Neutral electrolyte such as Na_2SO_4, NH_4Cl, for pH = 7 and
- Acid electrolyte such as H_2SO_4, for pH < 7

In general, aqueous electrolytes have lower ions transport resistance and a higher ionic concentration compared to ILs and organic electrolytes. Owing to smaller ionic radius and higher ionic concentration, EC containing aqueous electrolytes show higher power and capacitance than those with other types of electrolytes. Moreover, this electrolyte can be readily prepared without stringent preparation procedure and conditions unlike other electrolytes. However, an important drawback of aqueous electrolytes is their small operating voltage window which is around 1.2 V due to water decomposition, and this limits the improvement of both energy and power densities [6]. This can be reduced by finding a material with relatively high capacitance.

2.1.3 Advantages and Challenges of EC

Advantages

Compared to batteries, EC have many advantages such as:

(i) High power density:

Due to storing of electrical charges at the electrode surface and in the bulk near the surface of the solid in EC, the charge–discharge reaction is not limited by ionic transport into the bulk of the electrode materials; consequently the charging/discharging rates are significantly faster than the electrochemical redox reactions for battery materials. The high power density in EC is due to this quick rate. For example an EC can be fully charged or discharged in seconds (30 s), and the energy can be derived from it very quickly, within 0.1 s [37].

(ii) Long shelf life:

Unlike batteries, ECs can hold their capacitance and can be recharged to their original capacitance when left unused for a long period of time. However, self-discharge can still occur which causes the operating voltage to drop during this idling period [6,38].

(iii) Long life expectancy:

In batteries the electrochemical energy is stored by faradaic reactions, which frequently consist of irreversible phase alteration and irreversible inter conversion of the chemical electrode reagent, but in EC there are no or very small chemical charge transmission and phase alteration exists during charge and discharge cycles [6,39,40].

(iv) High efficiency:

EC have reversible charging and discharging processes during their comprehensive operational range of voltage, and the energy loss as heat throughout each cycle is relatively small and readily removed. It means that the cycle efficiency of EC is high (about 95%) even while operating at rates above 1 kW kg^{-1} [6,41].

(v) Environmental friendliness:

EC do not contain hazardous or toxic materials and the waste materials are simply disposed [6],

(vi) Safety:

In usual conditions, EC are much safer than batteries, in particular lithium-ion batteries [6],

(vii) Wide range of operating temperatures:

EC can function efficiently at tremendously high and low temperatures. The usual operational temperature for EC ranges from 40 to 70 °C [6].

Challenges

Beside their low energy densities, EC also suffer from high cost: The cost of raw materials and manufacturing continues to be major challenges for EC commercialization. This cost is related to the fabrication cost of the electrode materials. Presently, RuO_2 and carbon are the most commons electrode materials utilized in marketable EC and the price of high surface area carbon is still high not to mention the cost of the rare metal oxide [6].

2.1.4 Electrode materials

The capacitance of EC significantly relies on the specific surface area of the electrode materials. In general the entire specific surface area is not electrochemically accessible to the ions. This specific area is in general made of porous material with different pore sizes, which also influence the charge storage mechanism. For instance, pore size very close to ion size in an ionic liquid electrolyte, yielded maximum double layer capacitance [42].

2.1.4.1 Carbon materials

Carbon materials have many advantages such as abundance, good electronic conductivity, easy processing, great chemical stability, low cost, high specific surface area and wide operating temperature range [39]. Carbon materials store charges at the interface of the electrode and the electrolyte, instead of storing them in the bulk of the electrode material. Since the charges are stored on the surface of the electrodes, fast energy delivery is possible but with no contribution of the bulk of the electrode materials to the charge storage, low amount of charges are stored. In other words, these materials have high power density but low energy density. Thus, the first intuition will be to increase the useful specific surface areas (specific surface areas effectively used for storage) in order to augment the charge accumulation at the electrode/electrolyte interface, which should also increase the energy density of the electrode materials [43]. In addition, hybridizing the carbon electrode materials with additional electrochemically active materials should also enhance the specific capacitance and subsequently the energy density [6].

2.1.4.1.1 Allotropes of carbon

Carbon is actually a unique chemical element in the periodic table. It can form an extensive variety of architectures in all dimensions, both at the macroscopic and nanoscopic scales. New forms of carbon have been found, during the last 20 years. Nowadays, the family of carbon-based materials spreads from C_{60} to carbon nanotubes and from old diamond and graphite to graphene. The properties of these new forms of carbon are so striking that they may even redefine our time. Carbon is one of the versatile element in the periodic table in terms of the number of compounds it may produce, chiefly owing to the types of bonds it may form (single, double, and triple bonds) and the amount of diverse atoms it can connect in bonding. Carbon has $1s^2\ 2s^2\ 2p^2$ electronic configuration, in ground state (lowest energy). It has 2 core electrons (1s) that are not accessible for chemical bonding and 4 valence electrons (2s and 2p) that can take part in bond formation. In principle, the presence of 2 unpaired 2p electrons should only form two bonds from the ground state of carbon. However, it has the tendency to rearrange the configuration of these valence electrons; process called hybridization, where solely 2s and 2p electron are affected [44]. Thus three different hybridization of carbon are possible:

(i) sp^3 hybridization with mixing of the four atomic orbitals (one 2s orbital and three 2p orbitals) which leads to the formation of four sp^3 hybrid orbitals

(ii) sp^2 hybridization where three atomic orbitals mix (one 2s and two 2p orbitals) giving rise to three $2p^2$ hybrid orbitals.

(iii) sp hybridization where two atomic orbitals of the four (one 2s and one 2p orbitals) mix to form two sp hybrid orbitals, each filled with only one electron. The two remaining p orbitals which do not participate in the hybridization are perpendicular to each other.

These different hybridizations give rise to different allotropes of carbon with different characteristics. The first most commonly observed forms of carbon are diamond and graphite. Diamond has a sp^3 hybridization which results in a three-dimensional (3D) cubic structure. On the other hand, graphite is the sp^2 hybridized form of carbon. It contains only three bonds per carbon with the fourth valence electron in a delocalized state. This sp^2 structure gives rise to a planar two-dimensional (2D) hexagonal structure called graphene which when stacked together form the graphite layers [45,46]. The structure of diamond and graphite are depicted schematically in Figure 2.3.

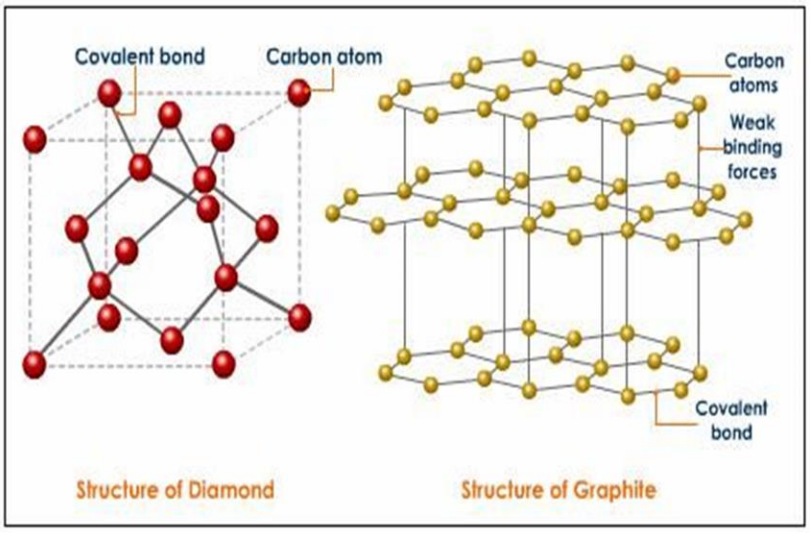

Figure 2.3: Structure of diamond and graphite [47]

This section will provide a brief overview of carbon nanomaterials and their potential use as electrode material for supercapacitor.

2.1.4.1.2 Carbon nanostructures

Carbon nanomaterials have a rich polymorphism of numerous allotropes displaying each possible dimensionality: fullerene molecule (0D), nanotubes (1D), graphite platelets and graphene ribbons (2D), and nano-diamond (3D) are some examples. Due to this unique versatility of nanomaterials exhibiting different physical and chemical properties, carbon nanostructures are playing a major role in nanoscience and nanotechnology [45]. The history of carbon nanoscience started with the discovery of C_{60} Buckminsterfullerene, by Kroto *et al.* [48].

(I) Fullerene and carbon nanotubes

Fullerene and carbon nanotubes (CNTs) were the first known nanocarbon allotropes with sp^2 hybridization. Fullerene (Figure 2.4 (a)) was discovered by Smalley and Kroto [48], in the mid-1980s with the common form being the C_{60}. It is basically a sheet of graphene specially wrapped in a certain direction. Such closed nanocarbon structures appear to be stable due to the high energy of dangling bonds at the edges of nano-sized graphene sheets. By adding carbon atoms to the basic structure of the fullerene, larger spherical or oblong structures are possible. In 1991, Iijima [49] discovered the single-walled CNTs (SWCNTs) which can be simply considered as a graphene sheet rolled up into a tube. Multi-walled CNTs (MWCNTs) can be seen as the Russian doll where a SWCNTs (Figure 2.4 (b)) are introduced into another SWCNTs with bigger diameter and so on [45,46].

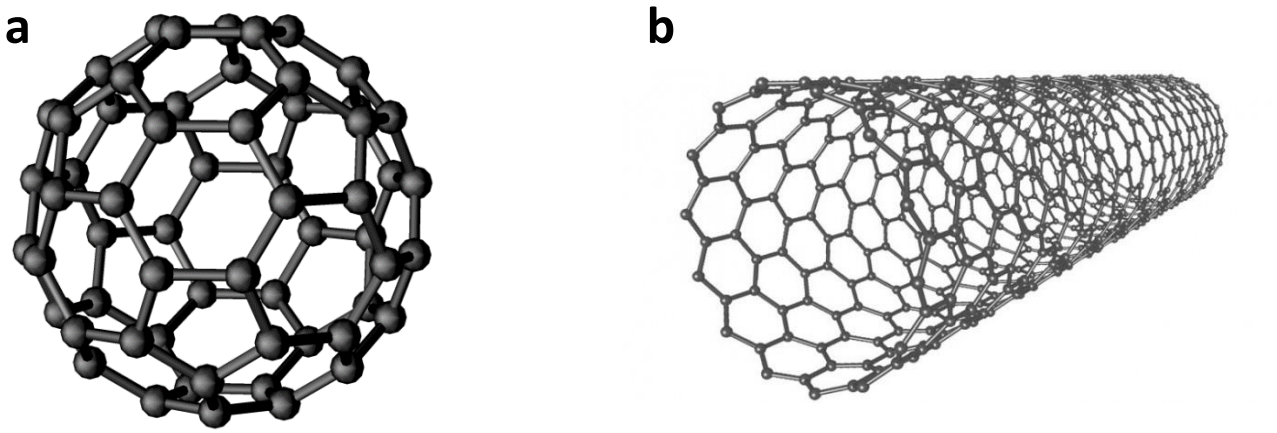

Figure 2.4: Structure of (a) fullerene [50] and (b) CNTs [51]

(II) Graphene

The planar layer of sp^2 bonded carbon atoms packed in a hexagonal honey comb crystalline structure is called graphene. Graphene is the thinnest material currently existing and can easily be obtained from graphite. Graphene is indeed the single layer version of graphite, hence graphene and graphite are intimately related [46,52].

In 2004, ground breaking research by Geim and Novosolov [53], (Nobel prize winner in physics 2010) from the University of Manchester showcased the accessibility of a single free-standing layer of graphene. Geim and Novosolov utilized scotch sticky tape to repeatedly peel sheets off bulk graphite layer until getting one layer of graphite called graphene (Figure 2.5) [46]. Recently, graphene has been synthesized using different methods which will be reviewed in the next section with a special focus on the chemical vapor deposition (CVD) method.

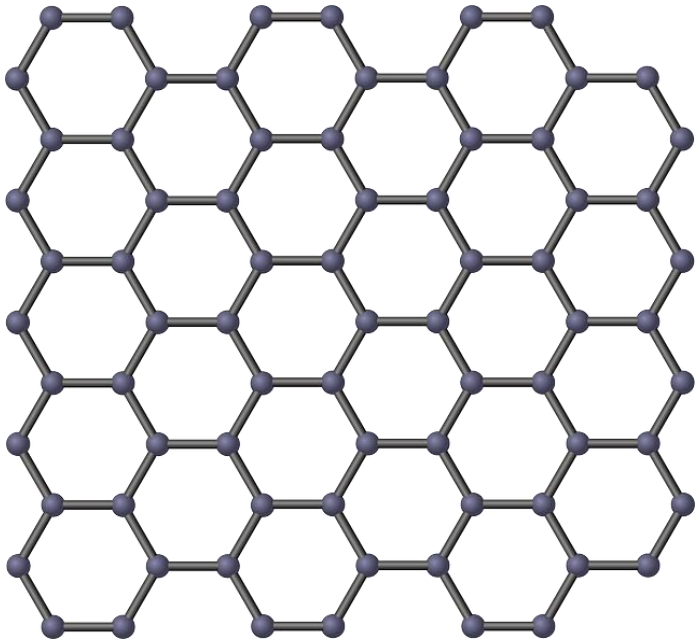

Figure 2.5: Structure of graphene [54]

1. Graphene Preparation

Here are some of the graphene preparation method: (1) Unzipping of CNTs [55], (2) arc-discharge method [56], (3) thermal reduction of graphene oxide into graphene [57], (4) chemical reduction of graphite oxide into graphene [58], (5) electrochemical preparation of graphene [59], (6) reduction of graphite oxide by laser radiation [60] and (7) chemical vapor deposition (CVD) method [61]

Chemical Vapor Deposition (CVD)

The technological viability of graphene-based electronic, optoelectronic, chemical- and bio-sensing devices depends on fabrication of large area and large scale materials of high quality. Catalytic chemical vapor deposition (CVD) is one of the few growth techniques available for the production of large area, high quality graphene thin films and foam. The main catalysts used are

Cu and Ni due to their facile etching by acid, large grain size and low cost [62–65]. Other metal such as Pt [66], Co [67] can be effectively used for catalyzing CVD graphene growth. Generally, during CVD of graphene, the precursor in a gas phase is sent into a reaction chamber, where it reacts with a catalyst at high temperature to subsequently form graphene. The precursor is typically a small hydrocarbon like methane or ethylene, but vaporized low-molecular-weight alcohols can also be utilized. The growth temperature ranges from several hundred degrees Celsius to the melting point of the catalyst metal. Depending on the catalyst, two principal mechanisms of graphene growth are suggested [64]: For polycrystalline Ni, the precursor is decomposed at the surface and carbon is dissolved in the metal catalyst, while with a Cu catalyst, carbon intermediate is not dissolved in the metal because of the insignificant solubility of carbon in copper (Cu) even at a very high temperature. Instead, the carbon atoms form graphene straight on the surface already at high temperature. The CVD on Cu is proposed to be self-limiting and surface mediated [64,68].

With the CVD procedures, 3D graphene network can be synthesized that could be used for energy storage applications. This original procedure makes use of Ni foam as metal template. The obtained porous graphene has a unique structure, similar to that of the Ni foam, allowing quick access of electrolyte ions because of its large surface area. Moreover, by directly synthesizing graphene onto a Ni foam acting as current collector, fast charge transfer from the active materials will be possible [69].

2. Properties of Graphene

Graphene has some unique structural and electronic properties which make it one of the most interesting materials. Electronic properties of graphene are very much dependent on the number of layers [70]. In general, graphene can be divided into three classes depending on the number of

layers: single-layer, bilayer and few-layer graphene, the latter referring to graphene with a layer number less than 10. Beyond this layer number, the carbon material can be considered as graphite since they both have similar electronic properties.

Some of the graphene properties are its large theoretical surface area of 2630 m^2 g^{-1} for graphene's single layer [18], its chemical stability and its impermeability to gases, its high electrical conductivity ($\sim 2 \times 10^3$ S m^{-1}) [17], high current density in the order of (10^8 A cm^{-2}) [71–73], high electron and hole mobilities at room temperature (230 000 cm^2 Vs^{-1}) [53], its outstanding mechanical properties with high strength (130 GPa) [74], it's extremely high Young modulus (1 TPa) [74] and large number of edge planes/defects. One of the most striking properties of graphene is its highly uncommon nature of charge carriers, which act as massless relativistic particles (Dirac fermion) [75,76]. At these Dirac points the valence and conduction bands are degenerated, making graphene a zero band gap semiconductor and suitable as an electronic material. These properties make graphene suitable for potential use in electrochemical field which denote a promising catalyst carrier in the next generation of carbon-based supports [77].

2.1.4.1.3 Carbon nanomaterial as electrode for supercapacitor

Carbon materials are futuristic electrode materials for industrial development. The benefits of carbon materials comprise lower cost, abundance, non-toxicity, easy processing, good electronic conductivity, high chemical stability, higher specific surface area and wide operating temperature range [39]. Carbon-based materials store charges primarily in an electrochemical double-layer layer at the interface between the electrolyte and the electrode, instead of storing them in the bulk of the capacitive materials. Consequently, the capacitance is mainly influenced

by the surface area available to the electrolyte ions. The significant parameters influencing their electrochemical performance are the pore-size distribution, the specific surface area, pore shape and structure, surface sufficiency and electrical conductivity. Between these, the most important factors that significantly affect the performance of the carbon materials are the pore-size distribution and specific surface area. In summary, carbon for EDLC should have three features: (1) high surface area, (2) good intra-and inter-particle conductivity in porous matrices, and (3) good electrolyte availability to the interpore area of carbon supplies [40]. Hence, in process of choosing supercapacitor electrode materials, the overall rule is to obtain an available and high specific surface area material with respectable electrical conductivity. High surface area carbon materials primarily consist of activated carbon [78], carbon nanotubes (CNTs) [79], template porous carbon [80] and graphene [81,82]. Carbon materials with high specific surface areas have a better ability for charge agglomeration at the electrolyte/electrode interface. Moreover surface functionalization can alter the electrochemical process of the carbon material [43,83–85].

- Graphene as electrode

Graphene has been considered as a potential electrode material for ECs. Nevertheless, only a specific capacitance value of about 262 F g^{-1} has been attained in aqueous electrolyte for a pure graphene-based supercapacitor [77,82]. This is due to the propensity of graphene sheet to restack through formation of strong π-π interactions between neighboring layers leading to substantial decrease in the accessible surface area and consequently in a lower specific capacitance values reported so far. To prevent the restacking and improve the electrochemical performance of graphene based electrode it is essential to functionalize graphene using chemical moieties like carbonyl and hydroxyl groups [86] or implant the graphene layers with pseudocapacitive and/or

faradic materials which eventually avoids the restacking of graphene, but also participate to the total capacitance of the electrode [87–89]. Numerous hybrid compounds of graphene or graphene oxide (GO) have been reported. Compound like graphene-metal oxide or -metal hydroxide [90], [91] and -polymer [92] have all been investigated.

2.1.4.2 Faradaic materials

A new kind of electrochemical capacitor was detected in RuO_2, called pseudocapacitor due to its faradic charge transfer reaction, in 1971 [93]. The overall prerequisites for metal oxide in EC applications are [6]:

(i) The oxides must be electronically conductive,

(ii) The metal can be in two or additional oxidation states,

(iii) The protons can without restrictions intercalate into the oxide lattice on reduction, permitting facile interconversion of $O^{2-} \leftrightarrow OH^-$.

Conway [40], has recognized three faradic mechanisms that can impact the capacitive electrochemical features, and these three mechanism happen because of different physical procedures and in different kinds of materials (see Fig 2.6) [31]:

(i) Underpotential deposition:

This happens when metals form a monolayer at a different metal's surface well above their redox potential. One typical instance of underpotential deposition is that of lead on the surface of a gold electrode [31,94].

(ii) Redox pseudocapacitance:

This happens when ions are electrochemically adsorbed onto the surface or near the surface of material with an associated faradic charge-transfer.

(iii) Intercalation pseudocapacitance:

This happens when ions intercalate into the tunnels or layers of a redox-active material accompanied by a faradaic charge-transfer with no crystallographic phase alteration [31]. The intercalation can occur in both aqueous and non-aqueous electrolytes and can be intrinsic or extrinsic to the material. Intrinsic pseudocapacitive materials show typical capacitive charge storage for an extensive range of particle sizes and morphologies. These are materials like RuO_2nH_2O [95], MnO_2 [96], NiO [97], and Nb_2O_5 [98], and extrinsic pseudocapacitive or Faradic-like-material can emerge through suitable material engineering (nano-sizing). No pseudocapacitance exists in the bulk on these materials. A good example of such material is $LiCoO_2$ [99]. In this dissertation, layered double hydroxides (LDHs) and LDHs/graphene composites will be considered as electrode material for energy storage applications.

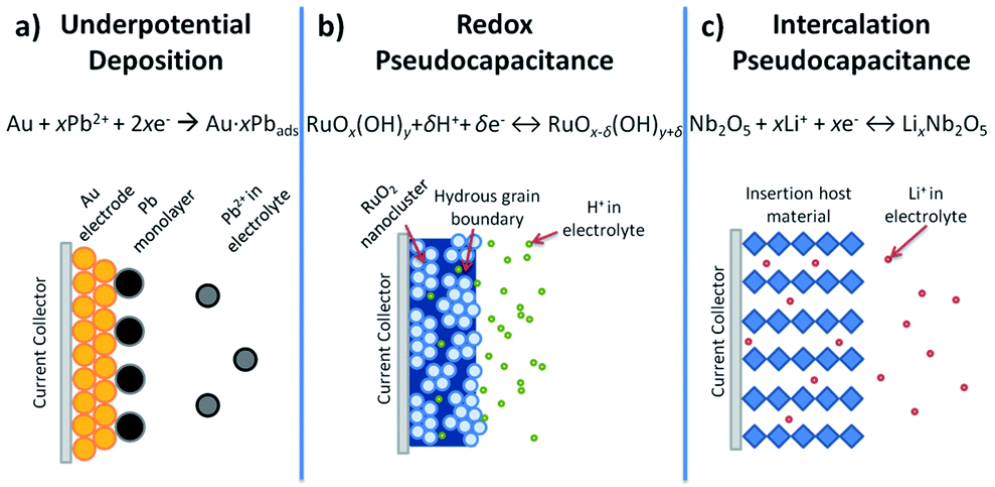

Figure 2.6: Different types of reversible redox mechanisms that give rise to pseudocapacitance: (a) underpotential deposition, (b) redox pseudocapacitance, and (c) intercalation pseudocapacitance [31].

2.1.4.2.1 Layered Double Hydroxides (LDHs)

Layered Double Hydroxides (LDHs) were discovered 150 years ago but it is only in 1915 that the stoichiometry of MgAl hydrotalcite was defined by Manasse [100]. The main structural specification of LDH was also only determined by Allmann and Taylor when using single crystal X-ray diffraction (XRD) in the 60s [101]. LDH is a category of 2 dimensional nanostructured inorganic materials. The common formula of LDH can be stated as [102]: $[M^{2+}_{1-x}\, M^{3+}_{x}\, (OH)_2]^{x+}$ $(A^{n-}_{x/n})$. mH_2O

With positively charged host layers of metallic hydroxide, where M^{2+} (divalent cation) could be Mg^{2+}, Ni^{2+}, Zn^{2+}, Co^{2+} , for example and M^{3+} (trivalent cation) may be Al^{3+}, Fe^{3+}, Cr^{3+}, etc. A^{n-} such as (CO_3^{2-}, NO_3^{2-}, Cl^-, OH^-, etc.) is the interlayer exchangeable hydrated anions which balances the specific positive charge, and m is the number of mole of water molecules located

with the anion in the interlayer space , and x is molar ratio $M^{3+}/(M^{2+} + M^{3+})$ ranging from 1.5 to 4.5. The three dimensional structure [103] of LDH is due to the electrostatic interfaces and hydrogen bond between sheets and the contents of gallery hold the sheets together,(see Fig 2.7) [102–104].

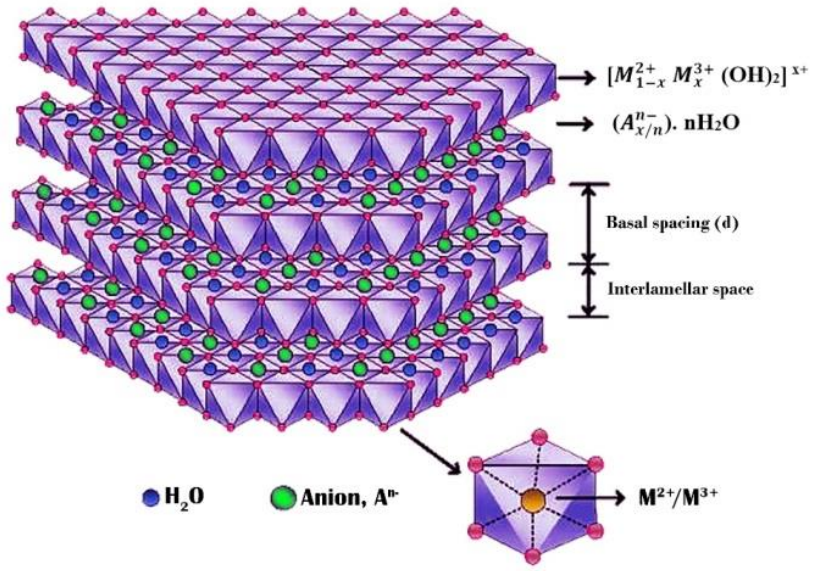

Figure 2.7: LDH structure [105]

The multiplicity of cations mixture like Ni^{2+}/Al^{3+}, Ni^{2+}/Mn^{3+}, Cu^{2+}/Cr^{3+}, Mg^{2+}/Cr^{3+}, Mg^{2+}/Fe^{3+}, etc., can be embedded in this hydrotalcites structure. If the anion does not produce a complex with the cations during the construction in the octahedral sheets, the number of anions is fundamentally infinite. Hence, the opportunity to make suitable materials for exact use is promising due to diversity of possible cations and anions mixture [106].

The main intrinsic properties of this class of materials are linked to their high layer charge density and their swelling abilities. LDHs have the advantage of being easily produced in large quantities in the laboratory through an economically viable process. With the fine-tuning of the

synthetic parameters, a tremendous variety of the chemical composition is possible, involving various metal cations and interlayer anions [107].

(I) Interlamellar anions

Anions, water molecules and occasionally other neutral or charged species are located in the interlamellar area of LDHs. One major characteristic of LDHs is that in most cases only weak bondings occur between these interlamellar ions or molecules and the host structure. Between the sheets, throughout creation of the lamellar structure, a great diversity of anionic types or additional anionic exchange can be present [108]. Within the layers, the subsequent anions can be established as follows:

- ✓ Halides (F^-, Cl^-, Br^-, I^-)
- ✓ Organic anions (CH_3COO^-, $C_2O_4^{2-}$, $C_6H_5COO^-$, etc.)
- ✓ Anionic polymers (PSS, PVS, Polyacrylate, etc)
- ✓ Anionic complexes of transition metals ($Fe(CN)_6^{2-}$, etc.)
- ✓ Oxo-and Polyoxometallate anions (VO_4^{3-}, CRO_4^{2-}, $V_{10}O_{28}^{6-}$, $CR_2O_7^{2-}$, etc.)
- ✓ Non-metal oxoanions (BO_3^{3-}, CO_3^{2-}, SO_4^{2-}, ClO_4^-, etc.)

It is more difficult to describe the construction of interlamellar area than the main sheets. In the X-ray diffractograms, an ordered stacking of the layers can be detected when LDHs comprising small anionic types like halides and carbonate with a base gap of 1.1 nm are present. With bulky anions, the X-ray diffractograms display only lines relevant to the base gaps and the construction of the main sheets [106,109]. Organic anions interact with the external hydroxyl groups creating hydrogen bond, whereas their hydrophobic hydrocarbon sequences are pushed away from the hydrophilic sheet surface [109,110].

In recent years two dimensional LDH nanosheets have been considered due to their unique physical attributes. For example, a quantum size effect corresponding to their ultra-thin structure which can turn them into building blocks for unique hybrid materials. For dissimilar anions, the priority of hydrotalcite is stated respectively as follows: $CO_3^{2-} > SO_4^{2-} > OH^- > F^- > Cl^- > Br^- > NO_3^- > I^-$ [111].

LDH composites with nitrate anions in the interlayer space are potential candidate for the slow-release of nitrate fertilizer due to their structure features [112].

(II) Synthesis of Layered Double Hydroxide

For the preparation of LDH, the main synthesis technique is the solvothermal method. This technique also has some variations such as the microwave assisted solvothermal.

- ✓ Solvothermal Method

One of the main methods for synthesis of inorganic materials is the solvothermal technique. The term hydrothermal is used when water is the solvent in the solvothermal process [39]. Hydrothermal method exploits the solubility of virtually all inorganic matter in water at high temperatures and pressures and subsequent crystallization of the soluble material from the solvent. The main role that water plays in the precursor material conversion at high temperature is due to its high vapor pressure and also the discrepancy in the water structure at room and high temperatures. The properties of the reactants, comprising their solubility and reactivity, further change at high temperature. These changes make available extra parameters to generate high-quality nanoparticles and nanocrystals, which are not possible at low temperature. Through the synthesis of nanocrystals, properties like water pressure, temperature, reaction time and the

respective precursor-product system can be tuned to keep up a high competitive nucleation and respectable size distribution [40]. The entire progression/growth happens in three stage procedures which consist of a fast nucleation of amorphous prime atoms, followed by crystal growth and final self-assembly. Over the course of reaction, the absorption of the reactants in the reaction medium is decreased and a chemical balance among the solid-liquid interface is proven. The small inner crystallites are still in a non-balance state. In this procedure, the external crystallites will serve as starting points to absorb the smaller metastable crystallites. Consequently, double hydroxide nanolayers progressively grow into their ultimate form. Numerous forces comprising the crystal-face interaction, the electrostatic forces, the Van der Waals forces and the hydrogen bonds contribute to this unique structure, [41]. Increasing trends of hydrothermal or solvothermal synthesis are profitable to the high-tech materials and biomolecules according to liquid nucleation mechanisms of hydrothermal or solvothermal procedures, dissimilar from the defusing appliances of solid-state reaction [39].

- ✓ Co-precipitation Method

It is one of the simplest and most used methods. This method is based on gradual increase of diverse solution of divalent and trivalent metal salt in a suitable ratio. A second solution is used to keep the pH to a desired value that leads to the co-precipitation of both metallic salts added to the reactor. The metal cations in the sheets of the material obtained are made of metal salt contained in the solution, but the origin of the interlamellar anion is still controversial. Co-precipitation methods achieve well-crystallized LDH but in some special cases, amorphous-like material is also possible. The main parameters that clearly affect the co-precipitation synthesis are: (i) temperature in the reactor, (ii) pH of the reaction medium, (iii) concentrations of metal

salt solution and alkaline solution, (iv) flow rate of reactants, and (v) ageing of the precipitate [109].

- ✓ Dehydration-rehydration (reconstruction) Method

In 1980, the reconstruction of the main LDH structure by hydration of the calcined LDH was defined by Miyata (the first one who describe it) [113]. This method is unique and is also called memory effect. At first, the LDH is calcined into a combination of oxides and then rehydrated in an aqueous solution containing selected anion to be intercalated. Temperature, ramping rate and duration of treatment are significant calcination conditions for defining structure recovery.

The lamellar structures of LDH can often be partly remade throughout the reconstruction step, achieving pure crystal-like intercalated structure, which can be tedious. The effective reconstruction and intercalation processes during this method rely on: (i) Reaction time, (ii) the configuration of the host sheet, (iii) the numeral and electronic structures of the anion [109].

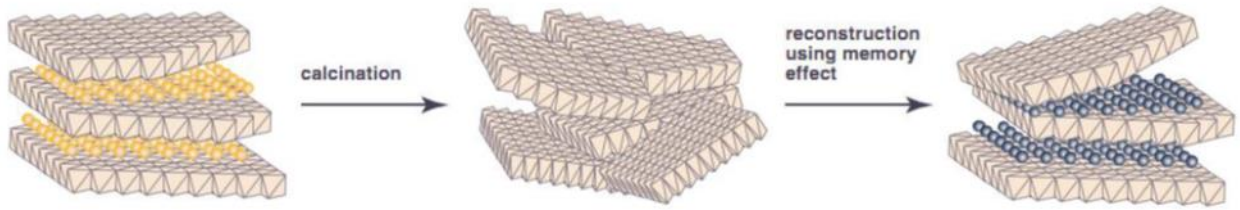

Figure 2.8: A simplified representation of the calcination/reconstruction method [108]

(III) Application of LDH

LDH has enticed considerable attention owing to its unique properties such as its adsorption capacity which is related to its relatively large surface area, its cation-exchange ability of the

Brucite layer, the anion-exchange of the interlayer space and the tunable basicity of the surface [114–116]. Hence, this material can be considered for bioactive nanocomposites due to its large surface area and also respectable thermal constancy. It can also serve as reaction media for photochemical and electrochemical processes [104]. It can be a host matrix for numerous organic anions and macromolecules [107]. It is also used as catalyst precursor, acid residue scavengers, flame retardants, stabilizer for polymers, in the medical fields, as antacids, antipeptides and stabilizer [26]. Unique structures are observed when LDH is used as precursors for metal oxides or magnetics materials. It is also an excellent electrode material for alkaline secondary batteries [34]. Recently, LDHs have shown potential in pseudosupercapacitor application owing to their high redox activity and relatively high capacitance [13,117]. In addition, due to their quantum size effect associated with their ultra-thin structure, they can become building blocks for unique hybrid materials [118].

- Application of LDHs as faradaic supercapacitor material

LDHs have many benefits for electrochemical use. Firstly, the divalent and trivalent metal atom can spread on the atomic level in a lamellar LDH flake with manageable constituents, creating electrochemical active metal atom with uniform spreading and tunable configuration. Secondly, delaminated LDH nanosheets not just display great electrochemical surface area but as well expose electrochemical active sites. In addition, LDHs thermal corrosion leads to the construction of layered double oxides (LDOs) by varied metal oxides or spinels as the main elements. High metal scattering, high surface area, manageable atom size and high thermal stability are some incomparable attributes of LDOs, all of which profit the creation of greatly stable and distributed electrochemical active metal. Several negatively charged majority guests

can be intercalated into the interlayer space of LDHs, creating LDH-based intercalated compounds by means of the anion exchange process of LDHs [9]. Scientists have shown interest in LDH consisting of transition metal ions as one of the electrode materials for supercapacitors because of their low cost, abundance and electrochemically active sites which produce EDLC and pseudocapacitance. Transition metal (Mn, Fe, Ni, Co, etc.) based LDHs have also higher redox activity which reflects in the higher specific capacitance obtained using these specific metals [119]. These transition metals based LDHs are environmentally friendly and relatively harmless to human being. In general, electrode materials for pseudocapacitors are transition metal oxide or hydroxide. The introduction of electrochemical active transition metal ions within LDH sheets at the molecular level can enhance the high spreading of transition metal, improving the redox activity (specific capability) of active materials, and also the structural solidity (cycle life) of electrode during the charge/discharge procedures. Thus, LDH consisting of transition metals are considered as one of the suitable electrode materials for high-performance Faradic capacitance. Table 1 compares the different specific capacitance for different LDHs containing transition metals.

Table 1: Compares the different specific capacitance for different LDHs containing transition metals.

Material	Synthesis Method	Electrolyte	Specific capacitance	Cycling stability	Ref
Hierarchical porous NiAl LDH	Solvothermal	6 M KOH	814 Fg^{-1} at 1.8 A g^{-1}	95% after 400 cycles at 18 A g^{-1}	[120]
Hollow NiAl LDH microsphere	Hydrothermal	1 M KOH	735 Fg^{-1} at 2 A g^{-1}	116.5 % after 1000 cycles at 8 A g^{-1}	[3]
NiAl LDH/G	Hydrothermal	1 M Na_2SO_4	96 Fg^{-1} at 4 A g^{-1}	100 % after 1000 cycles at 50 mVs^{-1}	[121]
NiAl LDH/GNS	Hydrothermal	6 M KOH	693 at 10 mV s^{-1}	122.5 % after 200 cycles at 10 mA cm^{-2}	[34]
CoAl LDH/G	Co-precipitation	6 M KOH	510 F g^{-1} at 5 mV s^{-1}	90% after 6000 cycles at 4 A g^{-1}	[122]
CoAl LDH/GO	Layered assembly	1 M KOH	1031 F g^{-1} at 1 A g^{-1}	100% after 6000 cycles at 20 A g^{-1}	[123]
CoAl LDH/GO	Microwave reflux	6 M KOH	772 F g^{-1} at 1 A g^{-1}	73% after 10,000 cycles at 6 A g^{-1}	[2]
NiAl/GNS LDH	Hydrothermal	6 M KOH	976 F g^{-1} at	99.2% after 500 cycles at 10 A g^{-1}	[124]
NiAl LDH/CNT/GNS	Solvothermal	6 M KOH	1562 F g^{-1} at 5 mA cm^{-2}	-	[125]
NiAl DHM/NF-G	Solvothermal	6 M KOH	1252 F g^{-1} at 1 A g^{-1}	-	[25]

In pristine LDH because of their low electrical conductivity and affinity to restack together in solid state preventing the ion accessibility to the surface of the LDHs, attempts have been made

to use carbon materials such as carbon nanotubes, carbon nanoparticle and graphene to improve the conductivity of the composite but also to prevent the restacking of the LDH [2,19,34,35]. Low power density and poor solidity of LDH are due to low electrical conductivity and the fast redox reaction. Four procedures have been considered to overcome these shortcomings. Firstly, composite of carbon material and LDH can increase the robustness of the composite as well as the power density of the electrochemical cell made from this hybrid material. Secondly, LDHs with higher interlayer area can be achieved by exchanging the interlayer anion, because the higher interlayer area permits extra electrolyte ions storage. Thirdly, by increasing the specific surface area, more active sites for electrochemical reaction are made available. Finally, by fabricating porous micro/nanostructures to ameliorate the mass transfer during redox reactions [126].

Chapter 3

3 EXPERIMENTAL PROCESSES AND CHARACTERIZATION METHODS

3.1 Synthesis of Graphene foam by Chemical Vapor Deposition (CVD) technique

Graphene foam was synthesized by a chemical vapor deposition (CVD) method, using a reaction assembly chamber consisting of a 2 inch diameter quartz tube enclosed in a furnace connected to flow-meters of different gas supplies. The gasses used for the graphene growth consist of argon (Ar, grade 5 - 99.999%), hydrogen (H_2, grade 5 - 99.999%) and methane (CH_4, grade 4.5 - 99.999%). Figure 3.1 shows the schematic diagram of the CVD system used in our work.

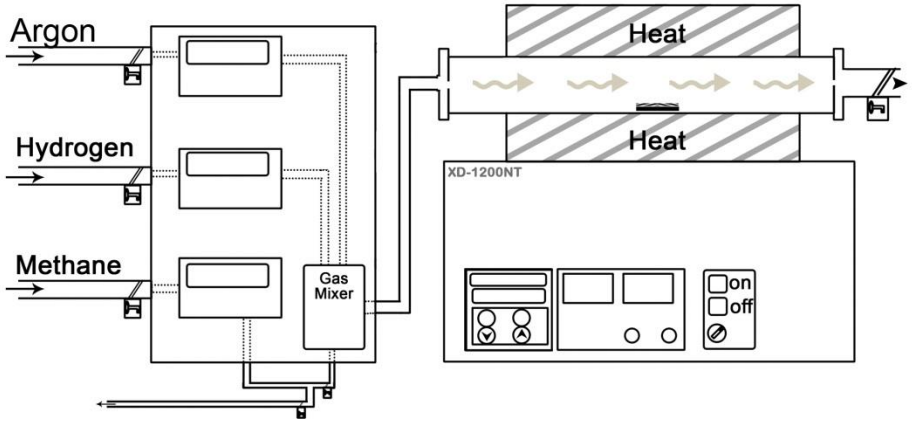

Figure 3.1: Schematic of the chemical vapor deposition system

CVD technique is a cost effective growth method for the production of relatively high quality, large yield graphene samples with exceptional electronic and optical properties necessary for device fabrication. Growth of graphene by CVD requires a metal substrate which acts as a catalyst to reduce the reaction's energy barrier. Typically, transition metals used for graphene growth are copper (Cu) and nickel (Ni). At elevated temperatures, nickel has comparatively high carbon solubility compared to copper. Consequently, multilayer graphene growth is only possible on Ni templates [127].

In this study, nickel substrate (Alantum, Munich, Germany) referred to as nickel foam (NF) with a 430 g m^{-2} area density and 1.8 mm thickness was utilized as a template for the growth of graphene at atmospheric pressure. During the growth process, gaseous precursors (Ar: H_2: CH_4) were fed into the reaction chamber via a gas mixer at specific flow rates. Decomposition of the gas mixture occurred as the gas passed over the hot reaction region of the furnace and the hydrocarbon precursor decomposes into carbon radicals on the metal substrate surface, creating single-layer, few-layer and multi-layers graphene [62,64,128]. Argon (Ar) gas served as the carrier gas to produce an inert environment while the hydrogen (H_2) gas worked as an eliminating agent to remove most of the oxide contaminations existing on the surface of the substrate material whilst increasing the grain size of the transition metal catalyst during the growth process [64].

Pristine Ni foam template was first cleaned by annealing at 800 - 1000° C for around 60 minutes in Ar/H_2 atmosphere to eliminate any kind of contaminations present. The annealing process also aids in enhancing the grain size for easy dissolution and out-diffusion of carbon atoms [64]. Thereafter, the hydrocarbon precursor (CH_4) gas was fed into the reaction chamber for a period of 25 – 60 minutes.

At the end, the obtained NF samples with carbon deposited on the surface were cooled down by a rapid cooling step which was achieved by pushing the hot end of the tube outwards, to a lower temperature area. Throughout the cooling process, carbon atoms diffuse out from the Ni-C alloy and precipitate onto the Ni surface to produce graphene films [65]. Based on the graphene growth mechanism on Ni, the cooling rate intensely affects the thickness and quality of synthesized graphene films. Fast and slow cooling rates give patches of graphene deposition on the Ni substrate but medium cooling rates result in the optimal carbon segregation and production of few layer graphene, as shown in Figure 3.2 [128]. Another significant factor affecting the nature of the synthesized graphene film morphology is the nickel foam's microstructure [65,128]. Subsequently, after the successful growth of graphene on the NF substrate, the nickel template was removed via a wet chemical etching process. Initially, the nickel foam-graphene (NF-G) was entirely soaked in 3.0 M hydrochloric acid and left for 20 hours. The final graphene foam sample without nickel present was finally washed with deionized water (DI) and dried in Ar/H_2 atmosphere.

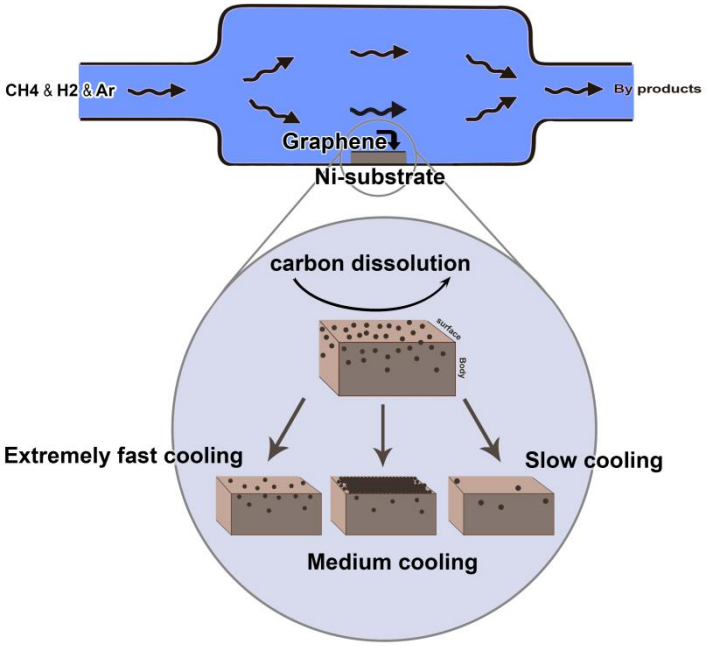

Figure 3.2: Image of the different cooling rates during graphene growth

3.2 Microwave method

Synthesizing organic materials using microwave irradiation is a relatively new method. The main advantages attributed to this method over other synthesis methods are significant reduction of reaction time and an increase in final material yield. As opposed to conventional heating for which the rate of heating is limited by the thermal conductivity of the container and the reactants, microwaves interact with individual molecules through two different mechanisms: Dipolar polarization and ionic conduction. Therefore, for material that are responsive to either of these mechanisms, immediate localized super heating of the reactants can be achieved using this method [129,130].

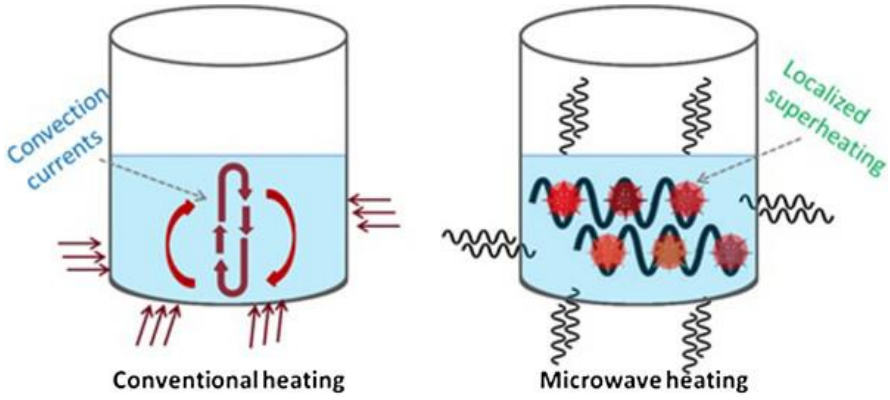

Figure 3.3: Graphical structure of heat introduction into a reaction mixture for conventional heating and microwave heating [131]

3.2.1 Principle of Microwave Heating

Microwaves are a group of waves in the electromagnetic spectrum whose frequencies range from 0.3 to 300 GHz. The energy transferred by these waves is usually not strong enough to cleave molecular bonds and can only create necessary thermal effects to provide activation energy for chemical reactions to take place. These thermal effects are created through two heating mechanisms that are unique to microwave technology [132]:

(I) Dipolar polarization:

When dipolar molecules are subjected to microwave irradiation, the negative and the positive poles of each molecule align themselves with the opposite charge within the microwave field and since the field is oscillating, the molecules constantly oscillate at the same frequency as the

microwave. This constant rotation and oscillation causes friction between the molecules resulting in heat generation [133–135].

(II) Ionic conduction:

Similar to dipolar polarization, ionic conduction is based on the interaction of a microwave field with free ions within a solution. When a solution containing negative and positive ions is irradiated with microwaves, these free ions move under the effect of the oscillating field and collide with each other. With every collision a small amount of heat is generated, [134,136,137]. It can clearly be understood that neither of these mechanism are affected by the thermal conductivity of the reactants or the container

3.2.2 Microwave induced nucleation and growth processes

The final shape and dimensionality of the resultant particles can be affected and controlled by a number of parameters such as reaction temperature, atmosphere, pressure, reaction time and precursor density. By careful manipulation of one or more of these factors, a variety of different nano-structures can be synthetized. There are four important steps that have to take place before and during the synthesis in order for the process to yield the intended final results. Each step is controlled by one or more of the mentioned variables. The first step is preparing and subjecting a solution containing necessary precursors and additives to microwave irradiation under controlled atmosphere, pressure and temperature. This step determines the structure and composition of the synthetized particles. The second step of the process takes place once synthesis is initiated. During this step, highly reactive intermediate species called “monomers” are generated within the solution. These monomers are responsible for the nucleation process. Once the generated

particles are thermodynamically stable, they will be allowed to grow to progressively larger sizes. This step is known as the growth process and is what determines the final size of the particles. The final step of the process involves dissolution of smaller sized particles due to Ostwald ripening which can take place depending on the reaction time. During this step, extra monomers are generated and grown to form larger sized particles. Setting up the parameters of the reaction in such a way that a balance between the nucleation and growth processes can be maintained, is the key to production of the correct particle type and size using microwave irradiation [128,138,139].

3.2.3 Synthesis of NiAl LDHs by Microwave-assisted hydrothermal technique

All chemicals used in this study were of analytical grade and were used as received without further purification. Initially, $Ni(NO_3)_2.6H_2O$ (Sigma-Aldrich, purity > 99.99%), $Al(NO_3)_3.9H_2O$ (Sigma-Aldrich, purity > 99.99%) and urea (Merck, purity ≥ 98%) were mixed together in 60 ml of deionized water to produce three aqueous mixtures with a Ni/Al ratio of 1.0, 2.0, and 3.0, respectively. The concentration of (Ni^{2+} + Al^{3+}) was kept at 0.1 mol/l and the molar ratio of $\frac{n_{urea}}{(n_{Al^{3+}}+n_{Ni^{2+}})}$ was kept at 2, (n is the mount of solute in moles).

A typical synthesis procedure uses a Ni/Al molar ratio of 2.0. In details, approximately 3.489 g of Ni^{2+} and 2.250 g Al^{3+} salts were added to DI water containing 0.960 g urea as shown in Figure 3.5. The solution was mixed and subjected to ultrasonic treatment for 10 minutes to ensure complete dispersion and dissolution of the salts. The mixture was then transferred into a 50 ml airtight quartz vessel and loaded into a microwave reactor (Anton Paar Synthos 3000 multimode reactor) operating with a 1400 W magnetron power and fitted with a wireless pressure and

temperature sensor. The microwave was operated at 400W. The sample temperature was ramped by 8° C/minute to a stable reaction temperature of 120° C and kept constant at this final temperature for a reaction time of 45 minutes with the pressure maintained at 80 bars during the holding time. Thereafter, the obtained product was filtered and washed several times with DI water and finally dried in an oven preset at 60° C for 10 hours.

Figure 3.4: Microwave used for synthesis [1]

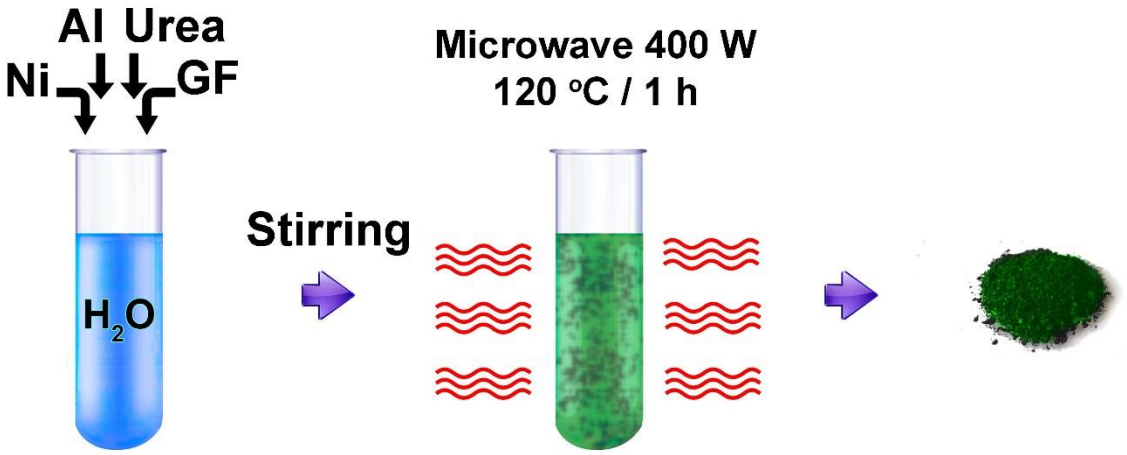

Figure 3.5: Synthesizes procedures

3.2.4 Synthesis of NiAl layered double hydroxide-graphene foam (NiAl LDH/GF) composites via microwave-assisted hydrothermal technique

In a typical synthesis procedure, 3.489 g of Ni^{2+} salt, 2.250 g Al^{3+} salt and 0.960 g of urea were mixed with different masses of graphene foam (10 mg GF, 15 mg GF and 20 mg GF) in 60 ml of DI water to produce three different aqueous solutions of NiAl LDH/GF. The mixture was then subjected to the same synthesis process as described above for NiAl LDH.

3.3 Electrode preparation

The process of electrode fabrication involved mixing 80 wt.% of the active material (NiAl LDH powder) or (NiAl LDH-GF powder) with 10 wt.% of carbon black (CB) and 10 wt.% of polyvinylidene difluoride (PVDF) binder in an agate mortar. A paste prepared from this combination was attained by addition of a few drops of 1-methyl-2-pyrrolidinone (NMP) to the

combination. The paste was then coated onto the surface of NF serving as the current collector. The coated samples were dried in an oven at 60° C for 12 h to ensure complete evaporation of the NMP.

3.4 Materials characterization

3.4.1 Morphological studies

(I) Scanning electron microscopy (SEM) technique

The most extensively utilized type of electron microscope is the scanning electron microscope (SEM) [140]. The scanning electron microscope records the observation and surface properties of heterogeneous organic and inorganic materials on a confined scale [141]. The electrons are produced from an electron gun and then accelerated through a set of deflector plates with electromagnetic lenses in an electron column to the sample surface. This is then used to inspect microstructures by scanning the surface of the materials at high resolution with a sensitive electron beam that scans over the surface area of sample thus producing the SEM image.

Characterization of the surface morphology and microstructure of the synthesized sample was done using a Zeiss Ultra Plus 55 field emission scanning electron microscope (FE-SEM) operated at 1.0 - 2.0 kV acceleration voltage, in secondary electron detection mode. Classically, the SEM samples were prepared by dissolving the powders in ethanol and dropping casting them on glass slides or double-sided tape attached to an aluminum substrate for analysis [25].

3.4.2 Structural and Qualitative phase studies

X-ray powder diffraction (XRD) method is an analytical method used to determine the crystal structure of materials and also to identify the phase of crystalline materials [140,142]. X-rays are created from high-speed electrons accelerated via a high-voltage field which bombard a metal target. The abrupt reduction in the speed of the electrons as it hits the target results in the conversion of the electron kinetic energy to x-ray radiation energy. To successfully generate the x-rays, an enclosed x-ray tube operated under vacuum with two metal electrodes and an electron source which provides a flux of electrons is required. A constant high voltage is kept across the electrodes to deflect the electrons to the anode target. The common targets generally used for generating x-rays are copper with wavelength of λ = 1.5406 Å or cobalt with wavelength of λ = 1.7890 Å. X-rays are generated in all directions as the electrons strike the target surface. Guiding windows are present to direct the x-rays to the desired location. A large amount of the electron kinetic energy is changed into heat and only a small amount is converted into x-rays. Thus, an efficient cooling system is required to cool down the entire x-ray tube [140].

X-ray diffraction methods are based on wave interaction phenomena which depend on the phase changes between two light waves which can either result in a constructive interference or destructive interaction. When a sample is bombarded with the x-rays, constructive interference of x-ray radiation occurs within the material as long as Bragg's law is satisfied (equation 6) [140,143]:

$$n\lambda = 2d \sin\theta \quad (6)$$

where λ is the wavelength, d is the distance between two atomic planes, θ is the angle between the incident beam and normal to the reflecting crystalline plane and *n* is an integer (i.e. 1, 2, 3.).

Investigation of the resulting XRD pattern is an ideal method for obtaining the different phases present in a material. The wavelength of the generated x-rays used is of the same order of magnitude as the interatomic spacing and bond lengths in crystalline solids (~ 1 Å).

The XRD spectra of all samples were obtained using an XPERT-PRO diffractometer (PANalytical, Netherlamds) operated with a Fe-filtered Co-Kα radiation of wavelength λ = 1.789 Å. The cobalt tube was operated at 35 kV and 50 mA with a scanning speed of 0.02^{o} per stage. The XRD patterns of all samples were recorded in the 2θ range of 5^{o} to 75.0^{o}. Qualitative phase analysis of the samples was conducted using the X'pert Highscore search match software.

3.4.3 Raman Analysis

One of the non-destructive techniques is Raman spectroscopy which is used to observe the rotational, vibrational and other low frequency modes in a material. It can also be utilized for determining the approximate number of graphene layers, and also check the quality of the synthesized graphene [144–146]. Raman spectroscopy technique is based on the inelastic scattering of monochromatic light, which is in general a source of laser line (emitting in the near ultraviolet or near infrared).

The laser light is absorbed by the material and interacts with phonons causing molecular vibration or other excitations in the specimen lattice which then result in shift in the transmitted photon wavelength, thereby providing information about the chemical and structural properties of the specimen. The wavelength of the transmitted photons is shifted up or down in relation to

the original wavelength of incident photons, which is called Raman effect [128]. The modes are directly related to the structural characteristics particularly in carbon based materials like graphite, graphene and carbon nanotubes due to the ease in assuming different hybridization states [147]. Raman spectroscopy also provides information about the crystallite size, on the in-plane vibration of sp^2 carbon atoms (G-band), disorder (D-band) and overtone (2D band), as well as on the crystallographic orientation of graphene doping [148,149].

In this work, the Raman spectra reported were recorded using a high resolution Jobin-Yvon Horiba T64000 micro-Raman spectrometer equipped with a triple monochromator system to remove the Rayleigh scattering. The samples were excited utilizing an argon excitation laser (of 514 nm wavelength) with a 15 mW power at the source. The laser was focused directly on the sample using a 50X objective with an acquisition time of 60 - 120 seconds per spectrum. Additional analyses of the recorded spectra were done using the LabSpec (Ver. 5.78.24) analytical software.

3.4.4 Fourier Transform Infra-red Resonance (FTIR) Spectroscopy

The Fourier transform infra-red (FT-IR) spectroscopy is a qualitative method used to investigate the unknown functional groups in a sample. It is a non-destructive technique which involves direct excitation of the specimen by an infrared (IR) radiation. Some part of IR radiation is absorbed (absorbance) while some part of the radiation passes through the sample (transmittance). Absorption, transmission or emission of the IR spectra is recorded over an extensive spectral range with the wavelength expressed as wavenumbers [150].

A Bruker Vertex 77v FT-IR spectrometer was utilized which was controlled by the Opus 7.0 spectroscopy software. FT-IR was used to detect the altered vibrational modes arising from the IR-excitation of the specimen. In addition, this method also gives information on the kind of the interlayer anions particularly in LDH and LDH/graphene composite materials [151,152]. For all measurements the wavenumber range was from 300 to 4000 cm^{-1}.

3.4.5 Gas Adsorption Analysis

Detailed information about the porosity, average pore volume, specific surface area and the overall pore size spreading of a material can be obtained by extensively analyzing the adsorption/desorption isotherms [11,121]. In this work, all of the experiments were done using a Micromeritics TriStar II 3020 (version 2.00) surface area and porosity analyzer. The Brunauer-Emmett-Teller (BET) method with nitrogen gas at 77 K was used to get the adsorption/desorption isotherms, specific surface area. Pore size and pore volume were subsequently obtained by adopting the Barrett-Joyner-Halenda (BJH) method from the desorption branch of the related isotherm [25]. Typical specific surface area measurements in this study were carried out by pre-heating the samples of known masses at 100° C under vacuum to eliminate adsorbed pollutants or moisture traces (usually carbon dioxide and water) from the atmosphere. This process is commonly referred to as the "degassing step". Thereafter, the degassed samples were loaded into the main analysis chamber for measurements at low temperature of -195° C. A specific amount of nitrogen is put into the sample with a subsequent withdrawal of the gas to obtain the quantity of gas absorbed by the sample over a relative pressure range, P/P_0 (i.e. $0.01 < P/P_0 < 1$). The pressure is allowed to stabilize after each dose of adsorption, and the amount adsorbed is calculated. The amount adsorbed for each pressure (and

temperature) describes an adsorption isotherm, for any amount of gas. With the area covered by each adsorbed gas molecule known, the specific surface area can be calculated [128,153]. The collected data is displayed in the form of a BET isotherm, which is a plot of the quantity of gas adsorbed as a function of the relative pressure (P/P_0). Analysis of the specific surface area was done by liquid nitrogen gas sorption at 77 K on a Micromeritics ASAP 2020 system.

3.4.6 Electrochemical Analysis

The electrochemical analysis was done using the cyclic voltammetry (CV) tests, galvanostatic charge/discharge (CD) and electrochemical impedance spectroscopy (EIS) tests controlled from a Biologic SP-300 PGSTAT workstation (Knoxville, TN 37930, USA). The SP-300 PGSTAT is controlled by the EC-Lab v10.37 software. The software monitors the applied potential difference to an electrochemical set-up including the working electrode (WE) with a current flow and reference electrode (RE) with no current flowing through. The potential difference between the working and the reference electrode is measured by the potentiostat. A potentiostat applies a current through the counter electrode (CE) and measures the current as an IR voltage drop [128,154].

The RE used was Ag/AgCl with a 3 M KCl filling solution and CE electrode was glassy carbon. Figure 3.6 shows the 3 electrode configuration setup. Information about the possibility of thermodynamic redox reactions of the working electrode (WE) are obtained from the CV curves and CD plots which give information about the mechanism of charge storage in addition to its capacitance retention ability. All these parameters rely on the shape of the plot and the time of the discharge at a continuous current density. The electrochemical impedance spectroscopy (EIS), done under stable condition was driven via a small amplitude AC sinusoidal signal of

potential or current in an extensive range of frequencies and the current or voltage response was measured.

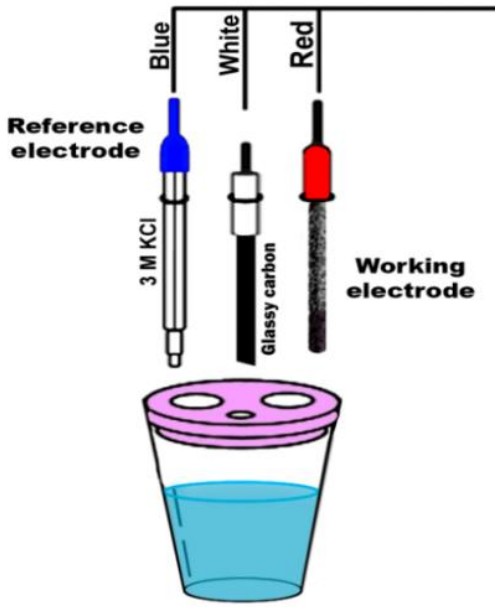

Figure 3.6: Three electrode set-up used for electrochemical testing of active materials electrodes. A reference electrode (blue), counter electrode (white), working electrode (red), are shown.

Chapter 4

4 Results and discussion

4.1 Characterization

4.1.1 Effect of Ni^{2+} and urea concentration on LDH's morphology

In order to improve the morphology of the LDH samples, The Ni^{2+} ion and urea concentrations were varied in order to keep the molar ratio $\frac{n_{urea}}{(n_{Al^{3+}}+n_{Ni^{2+}})} = 2$ during the hydrothermal synthesis. Figure 4.1 depicts the morphology of NiAl LDH samples prepared with the following parameters in 60 ml of water: sample 1 (Ni salt = 1.744 g, Al salt = 2.250 g, Urea = 0.720 g), sample 2 (Ni salt = 3.489 g, Al salt = 2.250 g, Urea = 0.960 g), and sample 3 (Ni salt = 5.234 g, Al salt = 2.250 g, Urea = 1.32 g). For sample 1 with the lowest Ni^{2+} content, non-defined shape is observed (Figures 4.1(a)-(b)). With the increase in the mass of the Ni^{2+}, the LDH structure evolved in well-defined flower-like structure as shown in Figures 4.1(c)-(d), for sample 2. With further increase in the mass of the Ni-salt, an intermediate morphology between sample 1 and 2 was observed. Mixture of flower like sheet and undefined structure are seen in the SEM micrograph of sample 3 (Figure 4.1(e)-(f)). The undefined structure may come from unreacted precursors which are in excess, namely Al salt for sample 1 and Ni salt for sample 3, during the synthesis process. Furthermore, the presence of Ni^{2+} ions seem to significantly influence the morphology of the sample since its deficit in sample 1 results in strongly undefined structure. The effect of deficit of Al^{3+} in the morphology of sample 3 is not as pronounced as Ni^{2+} deficiency in sample 1. The defined morphology is only obtained for sample 2. This structure is

obtained owing to a slow and homogeneous nucleation originating from the slow hydrolysis of urea [104]. Therefore, for the optimum production of uniformly distributed flower-like structure, the following masses of precursors will be used: Ni salt = 3.489 g, Al salt = 2.250 g, Urea = 0.960 g.

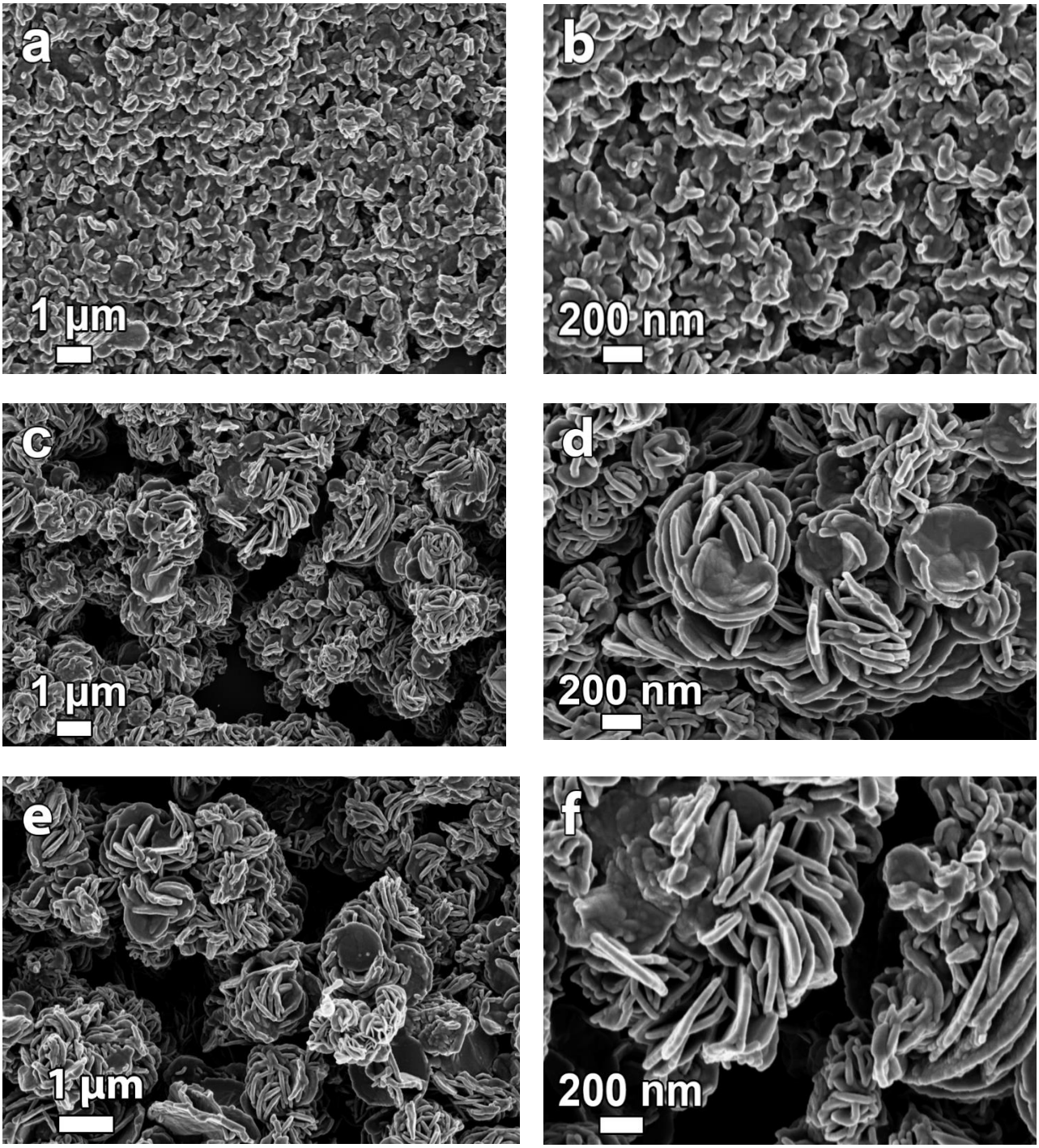

Figure 4.1: SEM images of NiAl LDH grown with the following parameters (a, b) Ni =1.744 g and Urea = 0.720 g, (b, c) Ni = 3.489 g and Urea = 0.960 g, (e, f) Ni = 5.234 g and Urea = 1.32 g

4.1.2 Effect of growth time on LDH's morphology

Figure 4.2 shows the SEM images of the LDH material produced (Ni salt = 3.489 g, Al salt = 2.250 g, Urea = 0.960 g) with different preparation times. Flower-like structure with similar sheet thickness is observed for all samples, regardless of the growth time. The results suggested that the growth time, from 1 to 5 hours, in the microwave-assisted hydrothermal synthesis, does not significantly influence the morphology of the sample. Based on this observation, one can assume that minimum growth time is enough to get good quality sample. However, other parameters such as the crystallinity, the surface area, need to be taken into account to confirm such assumption.

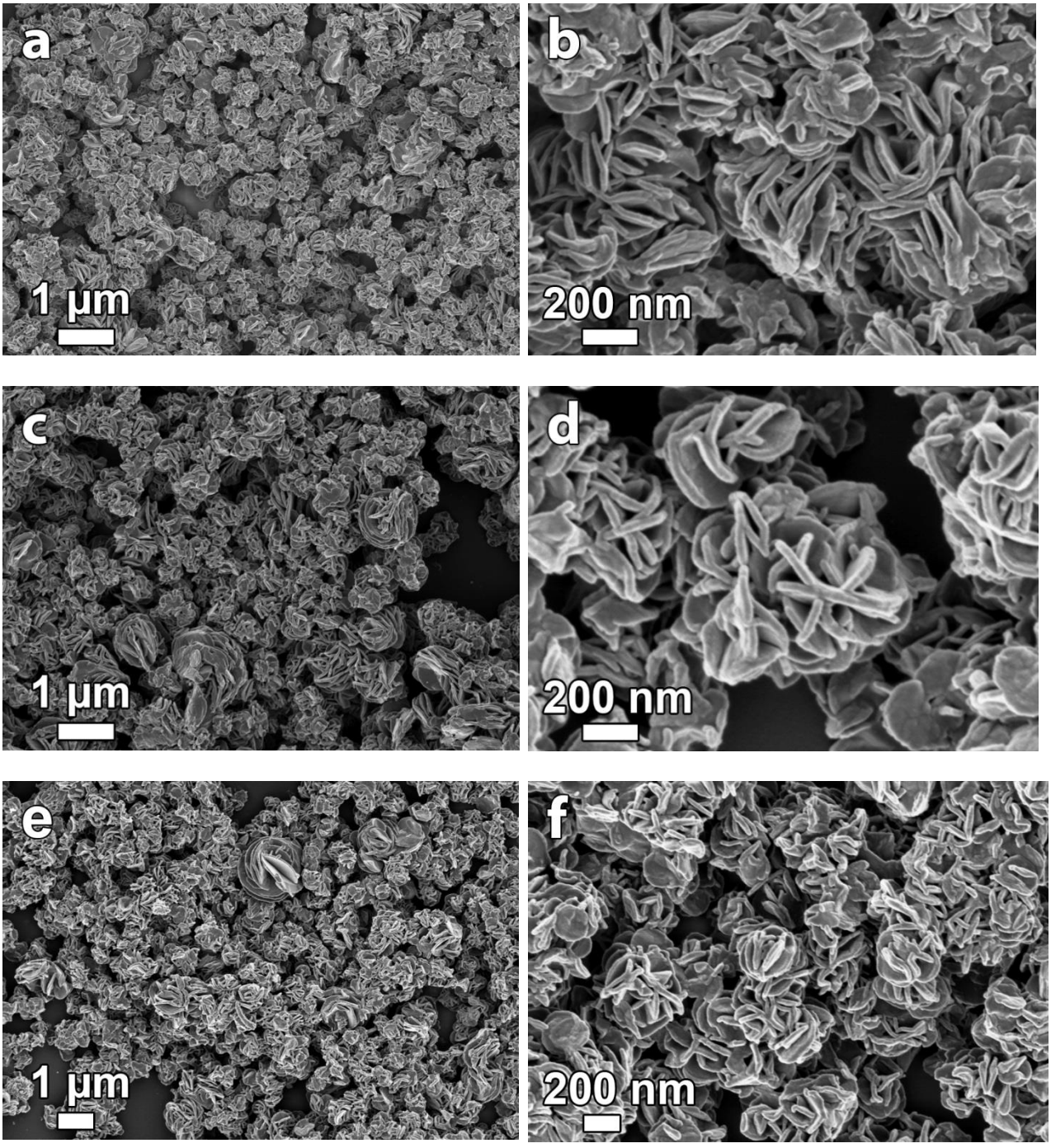

Figure 4.2: SEM images of NiAl LDH synthesized for (a, b) 1 hour, (c, d) 3 hours, and (e, f) 5 hours

4.1.3 SEM image of graphene

Figure 4.3 displays the SEM image of graphene foam at two different magnifications. The graphene layers display wrinkles and ripples due to the difference in thermal coefficients of Ni and carbon during the cooling step in the CVD synthesis.

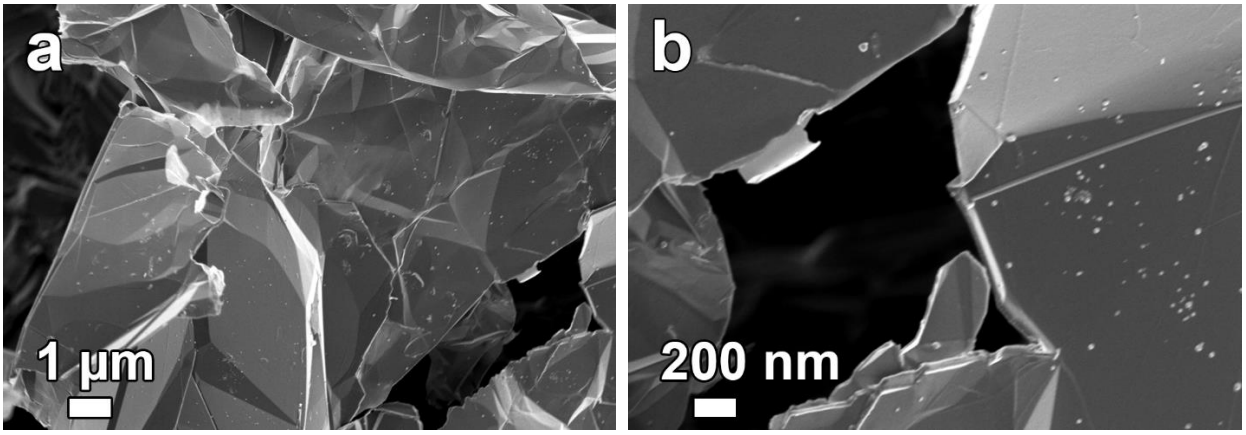

Figure 4.3: (a, b) SEM images of graphene at different magnifications

4.1.4 Effect of graphene mass loading on NiAl LDH/GF composite morphology

In order to improve the conductivity and possibly the exfoliation of the LDH material, different masses of graphene foam were dispersed in the LDH precursors prior to synthesis.

Figure 4.4 show the SEM micrographs for NiAl LDH/GF composites with different graphene mass loading. The growth parameters were those used for sample 2 with the only difference being the addition of graphene foam. The presence of graphene during the growth of the LDH does not change the flower-like morphology of the NiAl LDH. The micrographs also show an evidence of a partial growth of LDH on the graphene sheet. No significant decrease in the LDH thickness was observed regardless of the mass of graphene added.

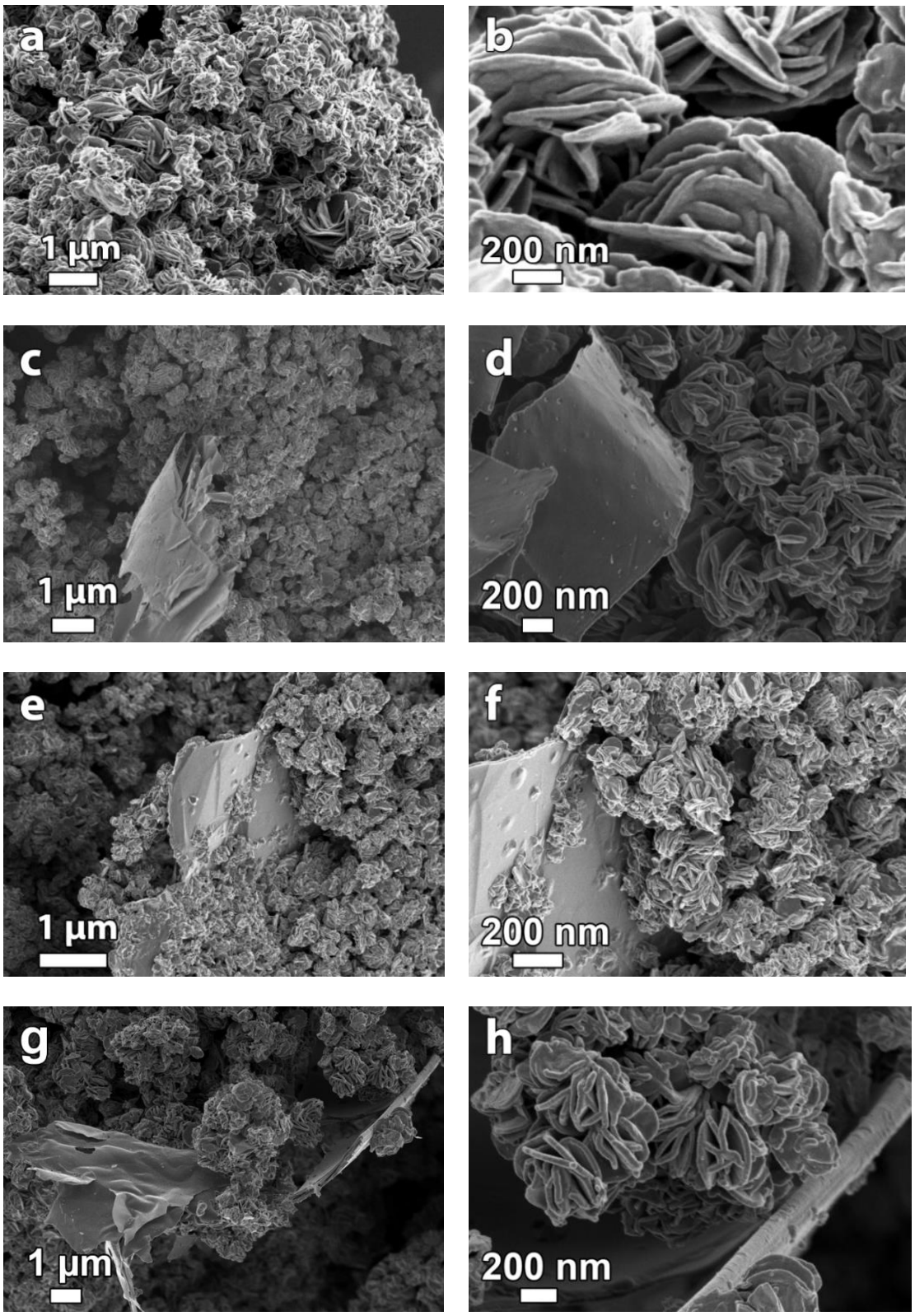

Figure 4.4: SEM images of (a, b) LDH, (c, d) LDH/GF (10 mg GF), (e, f) LDH/GF (15 mg GF), and (g, h) LDH/GF (20 mg GF) at different magnification.

4.1.5 XRD analysis of NiAl LDH and NiAl LDH/GF composites

Figure 4.5 compares the XRD pattern of the NiAl LDH with those of LDH/GF samples. The XRD pattern of NiAl LDH consists of five main peaks at 2θ values of 12.13°, 23.30°, 39.44°, 40.41°and 45.10° corresponding to the diffraction planes of (003), (006), (009), (015), (018), respectively [34,125,155]. These peaks can indeed be indexed to the hexagonal lattice with rhombohedral symmetry [26]. The sharp (003) peak hints at the creation of high crystalline and excellent structures of pristine LDH materials [125]. For the NiAl LDH/GF composites, an additional peak around 2θ = 25.23° appears. This peak is ascribed to (002) peak of graphitic materials [13,34]. The appearance of the (002) graphitic peak in the NiAl LDH diffraction pattern confirms the synthesis of the composite material. From equation 6, the d-spacing of the (003) and (006) diffraction peaks of the LDH are 0.71 and 0.38 nm, respectively. The d-spacing of the (003) and (006) planes are dependent on the charge and size of the charge-balancing interlayer anion. For CO_3^{2-} intercalated hydrotalcite clay, the d-spacing of the (003) and (006) planes are 0.78 and 0.39 nm, respectively [112]. These values are very close to the ones calculated in this work. This may suggest that the intercalated anion is CO_3^{2-}. Furthermore, the interlayer spacing of the graphene, calculated from the (002) peak position is 0.35 nm and it is a little larger than that of natural graphite (0.34 nm). This can be interpreted by the π – π stacking interplay among the graphene sheets [34].

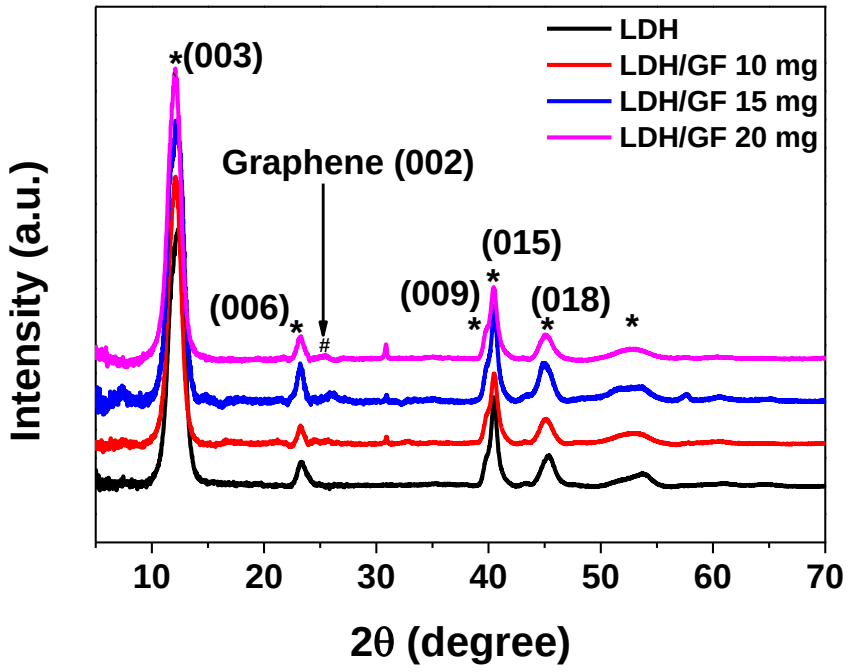

Figure 4.5: XRD diffraction patterns of LDH, LDH/GF (10 mg GF), LDH/GF (15 mg GF) and LDH/GF (20 mg GF)

4.1.6 FTIR studies of NiAl LDH and NiAl LDH/GF composites

In order to confirm the chemical composition of the grown materials, FTIR spectroscopy was used to study the vibrations in the octahedral lattice, hydroxyl groups and interlayer anion of the LDH sample. As shown in Figure 4.6, the infrared spectra of NiAl LDH and NiAl LDH/GF composites were done within the wavenumber range of 400 to 4000 cm^{-1}. The absorption band centered at about 3470 cm^{-1} corresponds to the O–H stretching vibration of the interlayer water molecules and the hydrogen-bonded OH-group of the hydrotalcite layers supplemented via the bending at 1634 cm^{-1}. The peak at 1341cm^{-1} originates from vibration of the interlayer CO_3^{2-} anions. The remaining bands at about 805 cm^{-1} and below are ascribed to metal-oxygen (M-O)/ metal-hydroxyl (M-OH) stretching modes [2,125]. Here, M corresponds to Ni and Al. In addition

to the bands related to the LDH structure, there is another band at around 2348 cm^{-1} that appeared when graphene was added to the LDH material. This band is tentatively assigned to graphene [25]. This confirms the XRD results from Figure 4.5 that NiAl/GF composites are successfully synthesized.

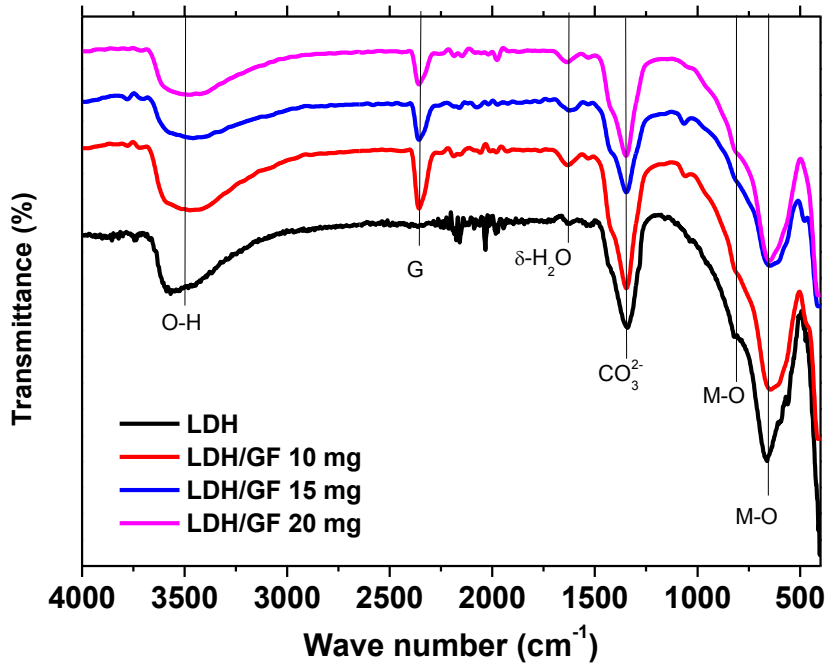

Figure 4.6: FTIR spectra of LDH, LDH/GF (10 mg GF), LDH/GF (15 mg GF) and LDH/GF (20 mg GF)

4.1.7 Raman spectroscopy of NiAl LDH and NiAl LDH/GF (20 mg GF)

Raman spectroscopy is useful in determining vibrational modes and type of bonding in materials [3]. Figure 4.7 displays the Raman spectrum of graphene, NiAl LDH and NiAl LDH/GF (20 mg.GF). In general, Raman spectrum of graphene consists of three main features: the D band

arising from the breathing mode with A_{1g} symmetry, observed at ~ 1350 cm^{-1} [19,125,156], and is normally associated with the defective structures [155], the G-band that arises from the first-order scattering of the E_{1g} phonon for sp^2 carbon atoms in the wavenumber range of 1500 - 1600 cm^{-1} and the 2D band involving two phonons of opposite momentum in the highest optical branch near the A_1 symmetry at K-point and observed at ~ 2700 cm^{-1}. For the NiAl LDH, the main vibrational modes are at ~ 555 cm^{-1} and 1046 cm^{-1}. They correspond to the hydroxyl layers and stretching mode of CO_3^{2-} [19,125,155]. In the spectra presented in Figure 4.7, in addition to the 2 main peaks related to NiAl LDH, three extra peaks at 482 cm^{-1}, 714 cm^{-1} and 1288 cm^{-1} are visible but their origins are not clear at this point. Our graphene foam spectrum only shows the G and 2D peaks. No D peak is visible, suggesting a high purity graphene was produced. For the NiAl LDH/GF composite, in addition to the graphene G and 2D peaks, 2 main Raman peaks related to NiAl LDH are also present. This indicates the coexistence of NiAl LDH and graphene [19,25,125]. Furthermore, the intensity of the 2D peak significantly decreases in the composite material. This peak is very sensitive to its environment and the interaction between the LDH and the graphene could be responsible for the decrease in intensity of the peak. However, this is not a conclusive assertion since the number of graphene layers produced might not be uniformly distributed and different Raman spectra could also arise from different spot.

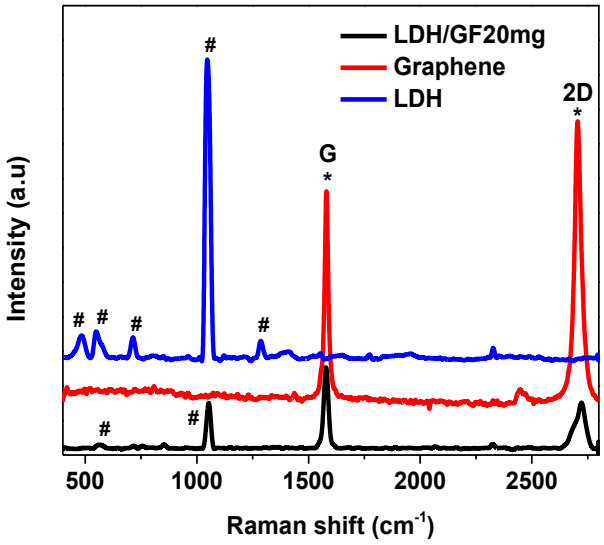

Figure 4.7: Raman spectra of graphene, LDH and LDH/GF (20 mg GF)

4.1.8 N_2 adsorption-desorption and BJH pore size distribution of NiAl LDH and NiAl LDH/GF composites

N_2 adsorption-desorption isotherms for all samples are presented in Figure 4.8 (a-d). The nitrogen adsorption-desorption isotherms show type III characteristics for all materials with H3 hysteresis, which is typical for vapor adsorption (i.e. water vapor on hydrophobic materials) and non-rigid aggregates of plate-like particles or assemblages of slit-shaped pores that show no saturation in the isotherm [157]. From these isotherms and using the BET theory, no significant increase in the calculated specific surface area of NiAl LDH and NiAl LDH/GF composites are observed (see table 2). Figure 4.8 (e) shows the pore size distribution of NiAl LDH and NiAl/GF composites. A small pore volume in all samples is located at ~ 4 nm (Figure 4.8 (e)), suggesting small amount of mesopores in these materials. High volume of macropore is indicated by the intense broad peak at around ~ 80 nm (Figure 4.8 (e)).

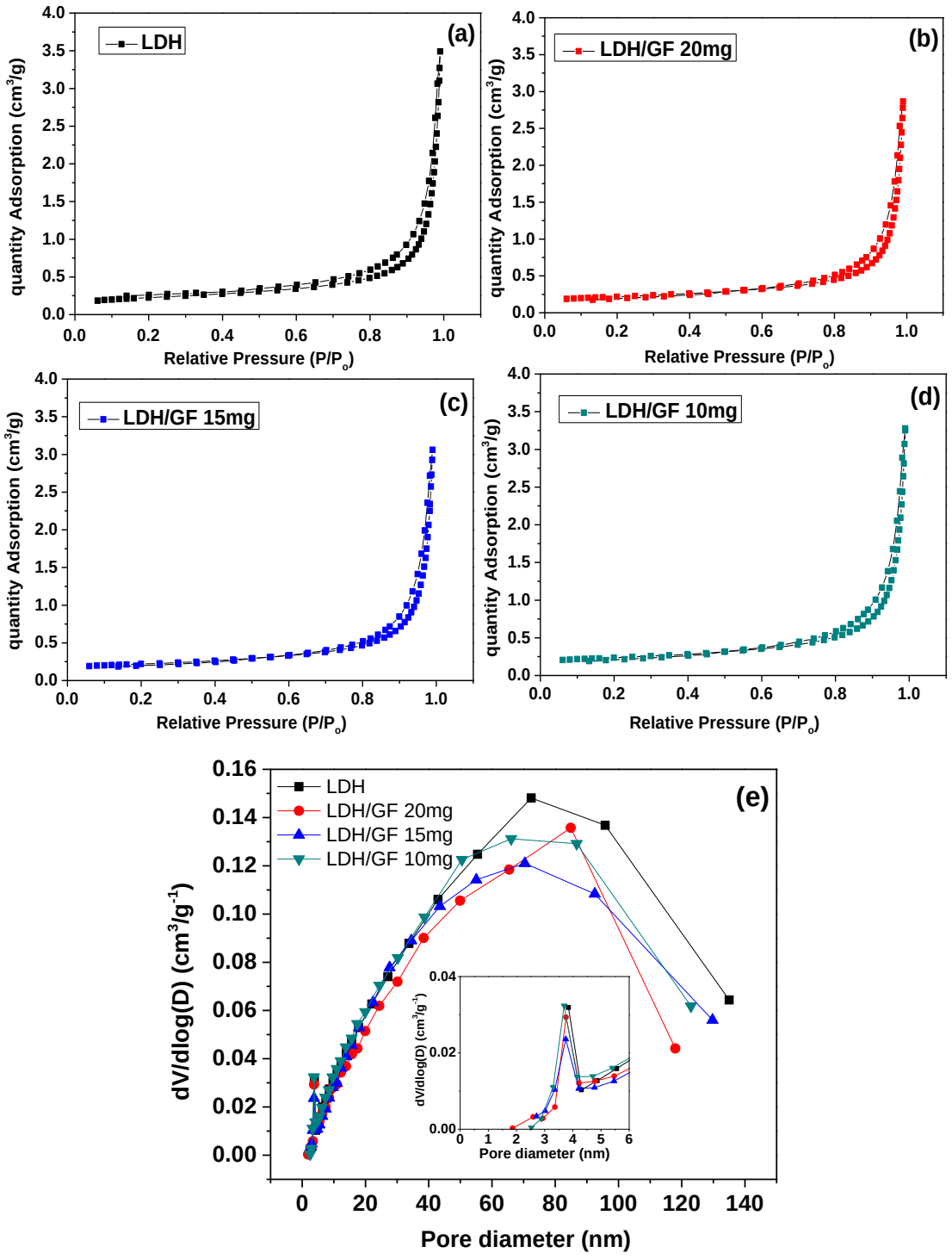

Figure 4.8: (a-d) N_2 adsorption-desorption isotherms loops for LDH, LDH/GF (10 mg GF), LDH/GF (15 mg GF), LDH/FG (20 mg GF), (e) BJH pore size distribution curves for corresponding samples.

Table 2: Surface area, micropore and cumulative volume and pore size of the samples

Sample	**Surface area (m^2/g)**	**Micropore volume[a] (cm^3/g)**	**Cumulative volume[b] (cm^3/g)**	**Pore diameter[c] (Å)**
LDH	16.7	0.002	0.120	279
LDH/GF 10 mg	17.1	0.004	0.114	242
LDH/GF 15 mg	15.7	0.004	0.106	254
LDH/FG 20 mg	15.7	0.003	0.099	243

[a] t-Plot micropore volume

[b] BJH Desorption cumulative volume of pores between 1.7 nm and 300.0 nm diameter

[c] BJH Desorption average pore diameter (4V/A)

4.2 Electrochemical characterization

4.2.1 Introduction

To investigate the potential use of the NiAl LDH and NiAl LDH/GF composites as faradaic electrode material for electrochemical capacitor applications, cyclic voltammetry (CV), galvanostatic charge/discharge (CP) and electrochemical impedance spectroscopy (EIS) measurements were performed. The NiAl LDH with abundant electroactive sites is expected to store energy via the redox based mechanism thus exhibiting faradaic behavior. As mentioned in chapter 2, the composite of NiAl LDH and graphene can take advantage of the synergistic properties of both materials, improving on the electrochemical properties of the composite material [13]. A 6 M KOH solution was used as the electrolyte for all electrochemical measurements.

4.2.2 Effect of scan rate

Figure 4.9 illustrates the CV curves for all samples at the scan rates of 5, 10, 20, 50, and 100 mV s^{-1}. The CV curves at a scan rate of 5 mV s^{-1} have a pair of redox peaks, observed at ~ 0.23 V (reduction reaction) and ~ 0.42 V (oxidation reaction), respectively. The appearance of these peaks indicates that the electrode reaction mechanism is based on faradaic behavior. The intensity of the redox peaks is not identical, indicating a quasi-reversible procedure [25]. This redox pair corresponds to the transition of altered oxidation states of Ni according to equation 7:

$$Ni(OH)_2 + OH^- \rightarrow NiOOH + H_2O + e^- \quad (7)$$

For NiAl/GF composites, shown in Figure 4.9 (b - d), the CV curves have comparable redox peaks (anodic peaks at about 0.2 V and cathodic peak around 0.4 V) like the redox pairs of pristine NiAl LDH. This implies the continuous faradic redox reaction of NiAl LDH is still

involved in the composite. At low sweep rates the electrolyte ions have enough time to diffuse into the pores/surface of the electroactive material. The CV curves, shows that an increase in scan rate (from 5-20 mV s^{-1}), shifts the cathodic and anodic peaks to the negative and positive potential respectively. This leads to an increased distance between the reduction and oxidation peaks. This phenomenon is mainly related of the resistance and polarization of the electrode [2]. The potential alteration ($\Delta E_{a,c}$) which represents the potential separation between the anodic and cathodic peaks, is utilized to study the reversibility of the electrochemical redox reaction: the greater the reversibility, the smaller $\Delta E_{a,c}$ [158]. In this work, $\Delta E_{a,c}$ values ranging from 90 to 110 mV obtained from the CV curves of all the samples is higher than the theoretical value of 59 mV, which confirms that the electrochemical reaction occurring at the electrode is not reversible, but rather quasi-reversible as explained above.

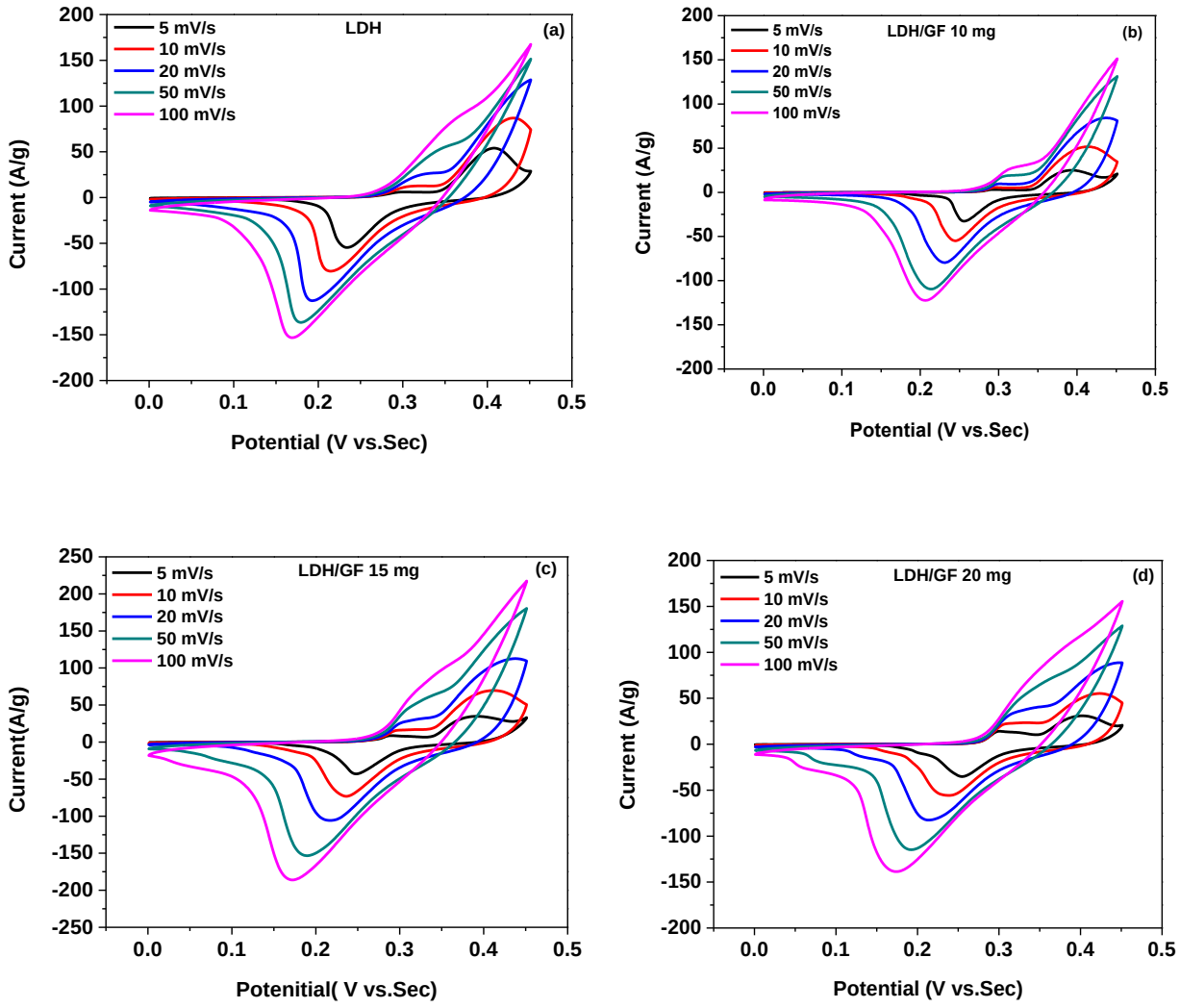

Figure 4.9: Cyclic voltammogram for (a) LDH, (b) LDH/GF (10 mg GF), (c) LDH/GF (15 mg GF), (d) LDH/GF (20 mg GF)

4.2.3 Comparative study of the electrochemical performance on NiAl LDH with different graphene loading.

Figure 4.10 (a) compares the CV for LDH and LDH/GF composites at 10 mV s^{-1}, while Figure 4.10 (b) shows the specific capacitance calculated from the CV curves of these samples at different scan rate, using equation 8 below:

$$C_s\left(\frac{F}{g}\right) = \frac{\bar{A}}{\upsilon m \Delta V} \quad (8)$$

In this equation $\bar{A}$ (mA V), is the integral area below the CV curve, υ (mV s^{-1}) is the scan rate, ΔV is potential window for each scan rate and m (g) is the mass of the active material.

From Figure 4.10 (a), similar CV curves for LDH and LDH/GF with 15 mg GF are observed. However, a close look at the curves shows a more distorted curve for the LDH sample. This implies that this sample shows higher resistance and subsequently weak stability upon the sweep rate. In addition, the LDH/GF with 15 mg GF electrode shows improved CV curve with high current response. This current response is associated with the optimized mass of GF and this is also supported by Figure 4.10 (b) where the highest specific capacitance for all sweep rates is obtained for LDH/GF with 15 mg GF.

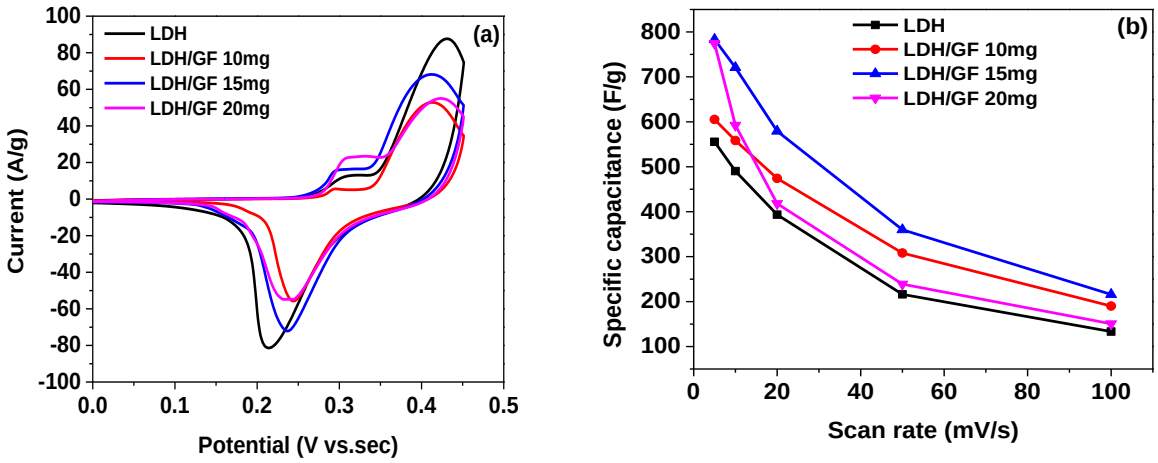

Figure 4.10: (a) cyclic voltammogram at sweep rate of 10 mV s^{-1} for LDH, LDH/GF (10 mg GF), LDH/GF (15 mg GF) and LDH/GF (20 mg GF), (b) Corresponding specific capacitance at different scan rates

4.2.4 Galvanostatic charge-discharge investigation of NiAl LDH and composites

Figure 4.11 displays the galvanostatic discharge of the LDH and LDH/GF samples at various current densities. All the samples presented a usual faradic. In other words, the discharge curves have two stages: from 0 to 0.35 V, a linear curve which stands for double layer capacitor, since the reaction of Ni^{2+}/Ni^{3+} doesn't happen under low voltage condition. The double layer behavior can be explained by the existence of partial charge adsorption at the interface between ions and electrode material [126]. The second stage involves two voltage phases: a quick potential drop (from 0.45 to 0.35 V) and a slow potential decay (from 0.35 to 0.2 V). The first one results from inner resistance, and the second one displays the faradaic attribute of the electrode [35]. There is clear alteration of the discharge curves from a straight line, which proves that the capacitance primarily comes from the faradic redox reaction [34]. The discharge times of the LDH/GF composites are longer than that of the LDH alone at the same current density and mass of active

materials. For example, the specific capacitance calculated from equation 9 below for NiAl LDH, NiAl/GF 10 mg GF, NiAl/GF 15 mg GF and NiAl/GF 20 mg GF composite electrodes are 897.7, 1204.5, 1616.2 and 1110.1 F g^{-1} at 5 A g^{-1} respectively.

$$C_{sp} = \frac{It}{m\Delta V} \quad (9)$$

In this equation, I is the current (A), t is the discharge time (s), ΔV is the voltage range (V) and m (g) is a mass of active materials, respectively.

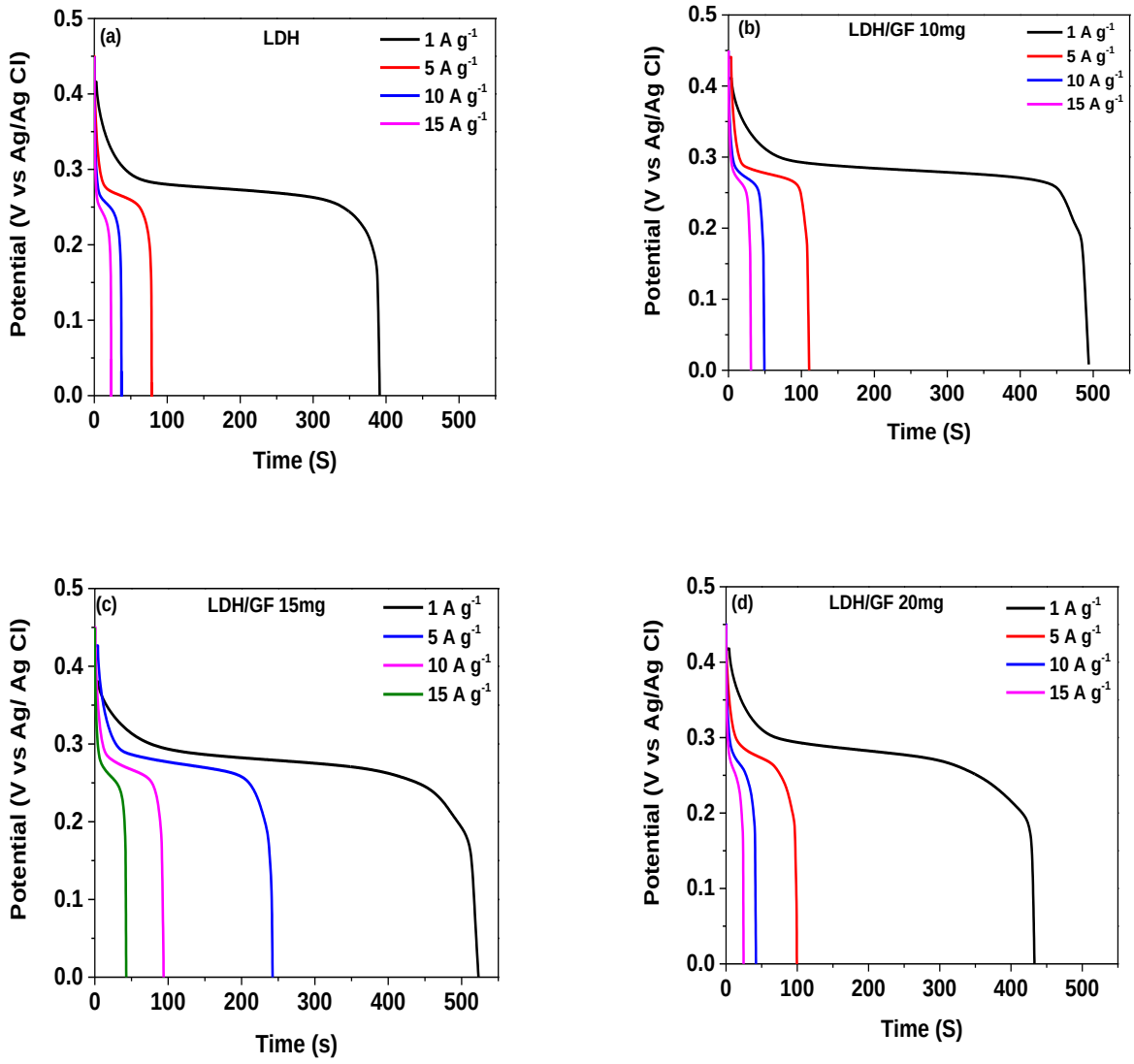

Figure 4.11: Galvanostatic discharge measured at different current densities for (a) LDH, (b) LDH/GF (10 mg GF), (c) LDH/GF (15 mg GF) and (d) LDH/GF (20 mg GF)

4.2.5 Dependence of specific capacitance of NiAl LDH/GF on graphene loading

Figure 4.12 (a) compares galvanostatic discharge measured for NiAl LDH and NiAl LDH/GF composites at current density of 1 A g^{-1}. The LDH/GF 15 mg electrode exhibits the highest discharge time. Figure 4.12 (b) shows the dependence of specific capacitance on the discharge

current densities for the different samples. In general, with the increase in current density, the specific capacitance of all samples gradually decreases. This is just due to the fact that only the exterior active surface is available for charge storage under extremely high current densities because of a reduced time for electrolyte dispersion and reaction. At a low current density, the electrolyte ions have adequate time to fully diffuse on the active material [35]. However, an ambiguous behavior is noticed at low current density for LDH/GF 10 mg GF and LDH/GF 15 mg GF. A steep increase in the specific capacitance is observed when the current density is increased from 1 to 5 A g^{-1}. This behavior is not well understood at this moment but might be due to the memory effect in this LDH/GF samples and also due to difference in charging potential at 1 A g^{-1}. Remaining ions stored in the inter-valley sites of the LDH during the lower current density sweep could contribute to the overall capacitance at higher current density. But this same behavior was supposed to be seen for the LDH and LDH/GF 20 mg GF, which is not the case here. The excellent electrochemical performance of the LDH/GF composites as electrode material for supercapacitor is due to the synergistic effect of faradaic NiAl LDH material with conductive graphene [13].

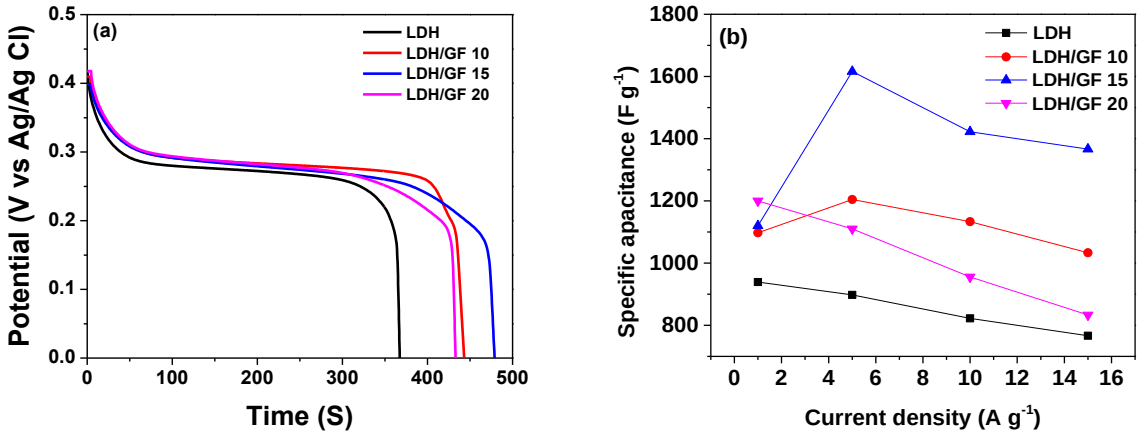

Figure 4.12: (a) Galvanostatic discharge measured at 1 A g^{-1} for LDH and LDH/GF composites, (b) specific capacitance of these electrodes at different discharge current densities.

4.2.6 EIS analysis of NiAl LDH and NiAl LDH/GF composites

EIS test was done in a frequency range of 10 mHz to 100 kHz at open circuit potential (E_{oc}) to evaluate the electrochemical performance of NiAl LDH and NiAl LDH/GF composites. Figure 4.13 (a) displays the Nyquist plot of NiAl LDH and NiAl LDH/GF composites. At high frequency, the curves show a deviation from the vertical line which indicates ideal supercapacitor. The smallest deviation is shown for the LDH/GF 15 mg GF sample, followed by LDH/GF 10 mg GF, LDH/GF 20 mg GF and LDH alone. The trend fits very well the behavior of the specific capacitance shown in Figure 4.12 (b), where the highest specific capacitance was observed for LDH/GF 15 mg GF sample with the smallest deviation from the vertical line while the smallest specific capacitance was obtained for the LDH sample which has the highest deviation from the vertical line. This deviation is due to leakage current and the more the deviation from the vertical line, the higher the leakage current which will consequently decrease the specific capacitance. In other words, the leakage current is sensitive to the diffusion

resistance of ions inside the electrode material [126]. The intercept on the x-axis of the Nyquist plot represents the solution resistance, R_s, which is the resistance related to the ionic conductivity of the electrolyte and electronic conductivity of the electrode and current collector [34]. From the EIS plot (Figure 4.13 (b)), the R_s values of the NiAl LDH and the NiAl LDH/GF (10, 15, 20 mg GF) composites are 0.49 Ω, 0.48 Ω, 0.47 Ω and 0.42 Ω respectively.

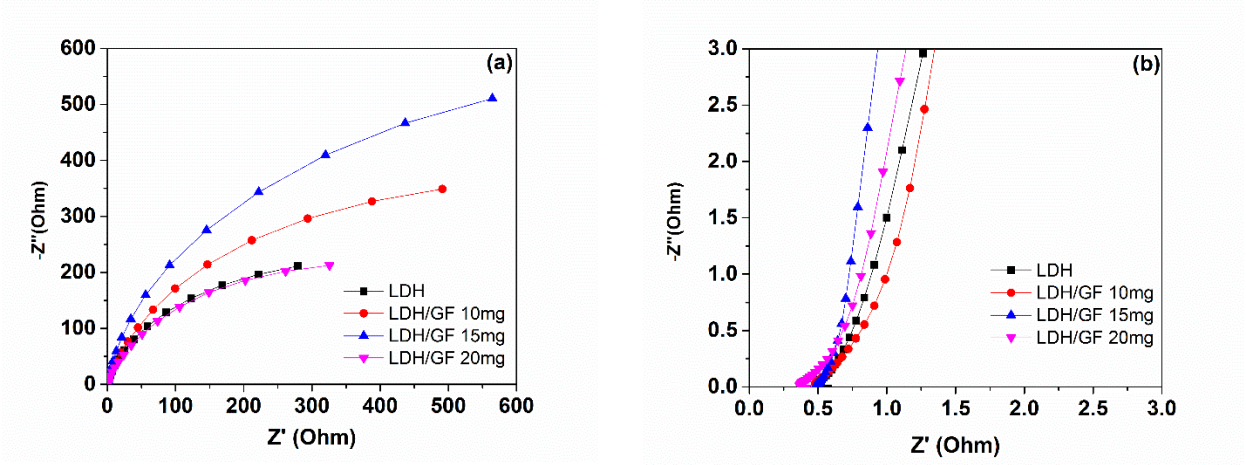

Figure 4.13: Nyquist plots of LDH, and LDH/GF composites (a) in full frequency range, (b) in low and high-mid frequency range (100 KHz – 10 mHz).

4.2.7 Fitting plot of NiAl LDH/GF with 15 mg GF loading

The fitting of the Nyquist spectrum data was performed for the best electrode, namely LDH/GF with 15 mg GF composite. A modified Randles circuit was employed with a set of resistors and capacitors in series and parallel using a fitting program ZFIT/EC-Lab version 10.40 and is presented as the inset to Figure 4.14. In the equivalent circuit of Nyquist plot of NiAl LDH/GF 15 mg GF electrode, R_S represents the solution resistance and is connected in series with a

constant phase element (Q) which indicates the presence of a double layer capacitance in the electrode. The high-mid frequency region is represented by the charge transfer resistance (R_{CT}) which is in parallel with the constant phase element (Q) and is in series with a mass capacitance (C_L), which is associated with the leakage current resistance R_L.

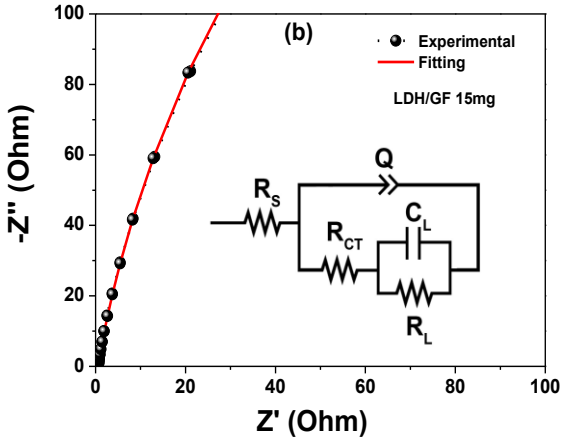

Figure 4.14: Fitting and stability of NiAl LDH/GF 15 mg GF

The fitting parameters are shown in table 3 and the value obtained for R_s is very close to the experimental value. Furthermore, the curve fits well with the plotted data. X^2 represents the criterion for minimization of the fit. $X/\sqrt{N}$, where N is the number of points and is a normalized expression of X^2. The error obtained with such expression is independent of the number of points [159].

Table 3: Fitting EIS parameters

Parameters	R_s (Ohm)	Q ($F.S^{(a-1)}$)	a	R_{CT} (Ohm)	C_L (F)	R_L (Ohm)	X^2	$X/\sqrt{N}$
LDH/GF 15 mg	0.47	5.882	0.875 9	0.572	2.267	876.4	0.024	0.025

4.2.8 Cycling stability of NiAl LDH and NiAl LDH/GF composites

Figure 4.15 displays stability of all samples for 1000 cycles. One can see that the LDH/GF with 15 mg GF electrode is more stable than the two other composites with coloumbic efficiency of 98% after 1000 cycles (see inset to Figure 4.15). The LDH alone shows fluctuation in the curve, suggesting variation of capacitance with each cycle.

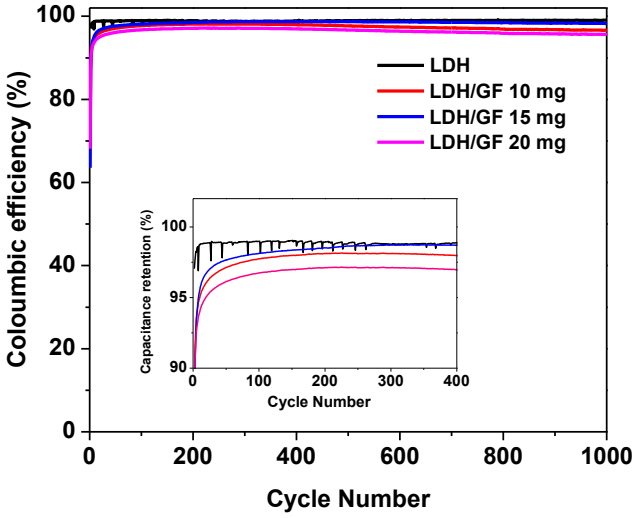

Figure 4.15: Cycling stability of LDH and LDH/GF composites for 1000 cycles.

4.3 Concluding Remarks

NiAl LDH and NiAl LDH/GF with different mass of GF (10, 15, 20 mg) were successfully synthesized by microwave assisted hydrothermal technique which significantly reduces the growth time of the conventional hydrothermal synthesis. SEM micrographs show sheet-like structure for the LDH structure. Good interaction of the LDH with GF in the composite was also observed. XRD measurements confirm the good crystallinity of the LDH and also the presence of graphene in the composite materials. Although no significant enhancement of the surface area was observed when GF was added to the composite, improved electrochemical performance were obtained. The CV, CD and EIS measurements showed that NiAl LDH/GF 15 mg GF has the best performance. This enhanced performance is ascribed to the addition of GF which improve the conductivity of the electrode material.

Chapter 5

5 GENERAL CONCLUSION

Chemical vapor deposition technique was used to produce unique 3D GF, which mimics the morphology of the nickel foam template used for the dissolution/diffusion of carbon atoms. The scanning electron micrographs, the morphology of graphene displayed wrinkles and ripples which are attributed to the difference in thermal expansion coefficient between the carbon and nickel during the cooling step in the CVD synthesis. A defect free structure of graphene was confirmed by Raman spectroscopy displaying only the G and 2D peaks, which are characteristic of carbon based materials. This structure is ideal for combination with different forms of suitable faradic-active materials. As a proof of the concept, NiAl LDH/GF was successfully synthesized using a facile microwave assisted hydrothermal technique which considerably reduces the growth time compared to traditional hydrothermal technique.

The SEM images, showed similar flower-like structure with similar thickness of the LDHs regardless the growth time. Thus, the minimum growth time of 1 hour was sufficient for the synthesis of good quality NiAl LDHs. Further optimization on the LDH structure shows that the best quality LDH sample could be obtained for the following salt concentration: Ni salt = 3.489 g, Al salt = 2.250 g, Urea = 0.960 g.

The LDH/GF composites demonstrate that the presence of graphene in the composites doesn’t change the flower-like morphology of NiAl LDH which grows uniformly on the surface of the graphene sheets.

XRD pattern of LDH was indexed to the hexagonal lattice with rhombohedral symmetry, showing high crystalline and excellent structure. Similarly, the XRD pattern of LDH/GF composites shows additional peak corresponding to the (002) peak attributed to graphitic material, confirming the homogeneous synthesis of the LDH/GF composites material. The d-spacing of the (003) and (006) diffraction peaks of the LDH are 0.71 and 0.38 nm, respectively which correspond very well with CO_3^{2-} intercalation.

The peak values of absorption bands corresponded to hydrogen bond, metal-oxygen, metal-hydroxyl and anions CO_3^{2-} FTIR vibrational modes, confirming the previous results of the successful synthesis of CO_3^{2-} intercalated NiAl-LDH.

In Raman spectroscopy results further confirmed the homogeneous synthesis of the NiAl LDH/GF composite with the observation of the NiAl- and graphene-related Raman vibrational modes in the composite material.

The nitrogen adsorption – desorption isotherms display type III characteristic with H3 hysteresis, hinting the presence of mesopore and macropore. A mesopore volume in all samples is located at ~ 4 nm and the macropore volume is located around ~ 80 nm. No significant change in the specific surface area for NiAl LDH and NiAl LDH/GF were seen.

CV studies showed that LDH/GF 15 mg GF has the highest current response and consequently the highest specific capacitance value of 724 F g^{-1} the specific compared to 484 F g^{-1} for pristine LDH at 10 mV s^{-1}. The composite with 15 mg graphene loading exhibited the highest discharge time with a specific capacitance of 1616 F g^{-1} compared to 897 F g^{-1} for pristine LDH at 5 A g^{-1}. Cycling stability of all samples after 1000 cycles showed that the LDH/GF with 15 mg graphene loading is more stable and hence, has the best electrochemical test responses.

No significant change in the R_s values obtained from the EIS plots for all samples was observed. However, EIS plots showed the smallest deviation from the vertical line for LDH/GF 15 mg, confirming the smallest leakage current for this electrode material. These improvements are a result of the addition of graphene foam to obtain a higher electrical conductivity for the composite.

In summary, by reducing the time and power, we save time and energy in producing LDH material and all the results have clearly demonstrated that incorporation of graphene in the LDH matrix to obtain a hybrid electrode significantly improved the electrochemical performance of hybrid electrode.

Reference:

[1] Microwave Synthesis - Synthos 3000 | Balkan Analytical, (n.d.). http://www.balkananalytical.com/29 (accessed September 30, 2015).

[2] J. Fang, M. Li, Q. Li, W. Zhang, Q. Shou, F. Liu, et al., Microwave-assisted synthesis of CoAl-layered double hydroxide/graphene oxide composite and its application in supercapacitors, Electrochim. Acta. 85 (2012) 248–255. doi:10.1016/j.electacta.2012.08.078.

[3] M. Shao, F. Ning, Y. Zhao, J. Zhao, M. Wei, D.G. Evans, et al., Core--shell layered double hydroxide microspheres with tunable interior architecture for supercapacitors, Chem. Mater. 24 (2012) 1192–1197.

[4] J.P. Zheng, The Limitations of Energy Density for Electrochemical Capacitors, J. Electrochem. Soc. 144 (1997) 2026. doi:10.1149/1.1837738.

[5] R. Kötz, R. Kötz, M. Carlen, M. Carlen, Principles and applications of electrochemical capacitors, Electrochim. Acta. 45 (2000) 2483–2498. doi:10.1016/S0013-4686(00)00354-6.

[6] G. Wang, L. Zhang, J. Zhang, A review of electrode materials for electrochemical supercapacitors, Chem. Soc. Rev. 41 (2012) 797–828.

[7] P. Vialat, C. Mousty, C. Taviot-Gueho, G. Renaudin, H. Martinez, J.C. Dupin, et al., High-performing monometallic cobalt layered double hydroxide supercapacitor with defined local structure, Adv. Funct. Mater. 24 (2014) 4831–4842. doi:10.1002/adfm.201400310.

[8] X. Zhang, H. Zhang, C. Li, K. Wang, X. Sun, Y. Ma, Recent advances in porous graphene materials for supercapacitor applications, RSC Adv. 4 (2014) 45862–45884. doi:10.1039/C4RA07869A.

[9] J. Wang, L. Wang, X. Chen, Y. Lu, W. Yang, Chemical power source based on layered double hydroxides, J. Solid State Electrochem. (2015). doi:10.1007/s10008-014-2723-5.

[10] J. Xu, S. Gai, F. He, N. Niu, P. Gao, Y. Chen, et al., A sandwich-type three-dimensional layered double hydroxide nanosheet array/graphene composite: fabrication and high supercapacitor performance, J. Mater. Chem. A. 2 (2014) 1022. doi:10.1039/c3ta14048b.

[11] A. Malak-Polaczyk, C. Vix-Guterl, E. Frackowiak, Carbon/Layered Double Hydroxide (LDH) Composites for Supercapacitor Application†, Energy & Fuels. 24 (2010) 3346–3351.

[12] L. Dai, J. Zhang, X. Wang, Y. Chen, The direct assembly of Mg–Al LDH nanosheets and

Mn(ii)–salen complex into sandwich-structured materials and their enhanced catalytic properties, RSC Adv. 3 (2013) 19885. doi:10.1039/c3ra42837k.

[13] Y. Wimalasiri, R. Fan, X.S. Zhao, L. Zou, Assembly of Ni-Al layered double hydroxide and graphene electrodes for supercapacitors, Electrochim. Acta. 134 (2014) 127–135. doi:10.1016/j.electacta.2014.04.129.

[14] J. Xiang, K. Kobayashi, M. Takahashi, G. Villemure, A. Yamagishi, Preparation of hybrid films of an anionic Ru (II) cyanide polypyridyl complex with layered double hydroxides by the Langmuir – Blodgett method and their use as electrode modifiers, Thin Solid Films. 397 (2001) 255–265.

[15] H. Li, L. Deng, G. Zhu, L. Kang, Z.H. Liu, Fabrication and capacitance of Ni2+-Fe3+ LDHs/MnO2 layered nanocomposite via an exfoliation/reassembling process, Mater. Sci. Eng. B Solid-State Mater. Adv. Technol. 177 (2012) 8–13. doi:10.1016/j.mseb.2011.09.012.

[16] X. Huang, X. Qi, F. Boey, H. Zhang, Graphene-based composites, Chem. Soc. Rev. 41 (2012) 666. doi:10.1039/c1cs15078b.

[17] Z.S. Wu, W. Ren, L. Gao, J. Zhao, Z. Chen, B. Liu, et al., Synthesis of graphene sheets with high electrical conductivity and good thermal stability by hydrogen arc discharge exfoliation, ACS Nano. 3 (2009) 411–417. doi:10.1021/nn900020u.

[18] M.D. Stoller, S. Park, Y. Zhu, J. An, R.S. Ruoff, Graphene-based ultracapacitors., Nano Lett. (2008) 6–10. doi:10.1021/nl802558y.

[19] J. Memon, J. Sun, D. Meng, W. Ouyang, M. a Memon, Y. Huang, et al., Synthesis of graphene/Ni-Al layered double hydroxide nanowires and their application as an electrode material for supercapacitors, J. Mater. Chem. A. 2 (2014) 5060–5067. doi:10.1039/c3ta14613h.

[20] J. Liu, Y. Li, X. Huang, G. Li, Z. Li, Layered Double Hydroxide Nano- and Microstructures Grown Directly on Metal Substrates and Their Calcined Products for Application as Li-Ion Battery Electrodes, Adv. Funct. Mater. 18 (2008) 1448–1458. doi:10.1002/adfm.200701383.

[21] E. Paek, A.J. Pak, G.S. Hwang, A Computational Study of the Interfacial Structure and Capacitance of Graphene in [BMIM][PF6] Ionic Liquid, J. Electrochem. Soc. 160 (2012) A1–A10. doi:10.1149/2.019301jes.

[22] K. Miyazaki, T. Abe, K. Nishio, H. Nakanishi, Z. Ogumi, Use of layered double hydroxides to improve the triple phase boundary in anion-exchange membrane fuel cells, J. Power Sources. 195 (2010) 6500–6503. doi:10.1016/j.jpowsour.2010.04.023.

[23] D. Kubo, K. Tadanaga, A. Hayashi, M. Tatsumisago, Improvement of electrochemical performance in alkaline fuel cell by hydroxide ion conducting Ni-Al layered double hydroxide, J. Power Sources. 222 (2013) 493–497. doi:10.1016/j.jpowsour.2012.08.093.

[24] M.M. Rao, B.R. Reddy, M. Jayalakshmi, V.S. Jaya, B. Sridhar, Hydrothermal synthesis of Mg-Al hydrotalcites by urea hydrolysis, Mater. Res. Bull. 40 (2005) 347–359. doi:10.1016/j.materresbull.2004.10.007.

[25] D. Momodu, A. Bello, J. Dangbegnon, F. Barzeger, F. Taghizadeh, M. Fabiane, et al., Solvothermal synthesis of NiAl double hydroxide microspheres on a nickel foam-graphene as an electrode material for pseudo-capacitors, AIP Adv. 4 (2014) 097122. doi:10.1063/1.4896125.

[26] Z. Yang, K.M. Choi, N. Jiang, S.E. Park, Microwave synthesis of hydrotalcite by urea hydrolysis, Bull. Korean Chem. Soc. 28 (2007) 2029–2033. doi:10.5012/bkcs.2007.28.11.2029.

[27] G.A. Tompsett, W.C. Conner, K.S. Yngvesson, Microwave synthesis of nanoporous materials, ChemPhysChem. 7 (2006) 296–319.

[28] X. Hu, J. Gong, L. Zhang, J.C. Yu, Continuous size tuning of monodisperse ZnO colloidal nanocrystal clusters by a microwave-polyol process and their application for humidity sensing, Adv. Mater. 20 (2008) 4845–4850. doi:10.1002/adma.200801433.

[29] H.M. a. Hassan, V. Abdelsayed, A.E.R.S. Khder, K.M. AbouZeid, J. Terner, M.S. El-Shall, et al., Microwave synthesis of graphene sheets supporting metal nanocrystals in aqueous and organic media, J. Mater. Chem. 19 (2009) 3832. doi:10.1039/b906253j.

[30] D.A.C. Stuerga, P. Gaillard, Microwave athermal effects in chemistry: A myth's autopsy. Part II: Orienting effects and thermodynamic consequences of electric field, J. Microw. Power Electromagn. Energy. 31 (1996) 101–113.

[31] V. Augustyn, P. Simon, B. Dunn, Pseudocapacitive oxide materials for high-rate electrochemical energy storage, Energy Environ. Sci. 7 (2014) 1597. doi:10.1039/c3ee44164d.

[32] P. Simon, Y. Gogotsi, B. Dunn, Where do batteries end and supercapacitors begin?, Sci. Mag. 343 (2014) pp–1210.

[33] B.E. Conway, V. Birss, J. Wojtowicz, The role and utilization of pseudocapacitance for energy storage by supercapacitors, J. Power Sources. 66 (1997) 1–14.

[34] Z. Gao, J. Wang, Z. Li, W. Yang, B. Wang, M. Hou, et al., Graphene nanosheet/Ni2+/Al3+ layered double-hydroxide composite as a novel electrode for a supercapacitor, Chem. Mater. 23 (2011) 3509–3516. doi:10.1021/cm200975x.

[35] M. Li, J.P. Cheng, J.H. Fang, Y. Yang, F. Liu, X.B. Zhang, NiAl-layered Double Hydroxide/Reduced Graphene Oxide Composite: Microwave-assisted Synthesis and Supercapacitive Properties, Electrochim. Acta. 134 (2014) 309–318. doi:10.1016/j.electacta.2014.04.141.

[36] R. Kötz, S. Müller, M. Bärtschi, B. Schnyder, P. Dietrich, F.N. Büchi, et al., Supercapacitors for peak-power demand in fuel-cell-driven cars, in: ECS Proc., 2001: pp. 2001–2021.

[37] A. Kusko, J. DeDad, Stored energy-Short-term and long-term energy storage methods, Ind. Appl. Mag. IEEE. 13 (2007) 66–72.

[38] A. Burke, Ultracapacitors: why, how, and where is the technology, J. Power Sources. 91 (2000) 37–50.

[39] Y. Zhang, H. Feng, X. Wu, L. Wang, A. Zhang, T. Xia, et al., Progress of electrochemical capacitor electrode materials: A review, Int. J. Hydrogen Energy. 34 (2009) 4889–4899.

[40] B.E. Conway, Electrochemical supercapacitors, (1999).

[41] J.R. Miller, A.F. Burke, Electrochemical capacitors: challenges and opportunities for real-world applications, Electrochem. Soc. Interface. 17 (2008) 53.

[42] C. Largeot, C. Portet, J. Chmiola, P.-L. Taberna, Y. Gogotsi, P. Simon, Relation between the ion size and pore size for an electric double-layer capacitor, J. Am. Chem. Soc. 130 (2008) 2730–2731.

[43] E. Frackowiak, Carbon materials for supercapacitor application., Phys. Chem. Chem. Phys. 9 (2007) 1774–85. doi:10.1039/b618139m.

[44] L.E.F.F. Torres, S. Roche, J.-C. Charlier, Introduction to graphene-based nanomaterials: from electronic structure to quantum transport, Cambridge University Press, 2014.

[45] L.E.F.F.O.A. TORRES, S. ROCHE, Introduction to Graphene-Based Nanomaterials (additional material), (n.d.).

[46] N.A. Koratkar, Graphene in Composite Materials: Synthesis, Characterization and Applications, DEStech Publications, Inc, 2013.

[47] Carbon Compounds | Chemistry@TutorVista.com, (n.d.). http://chemistry.tutorvista.com/organic-chemistry/carbon-compounds.html (accessed October 2, 2015).

[48] H.W. Kroto, J.R. Heath, S.C. O'Brien, R.F. Curl, R.E. Smalley, C 60: buckminsterfullerene, Nature. 318 (1985) 162–163.

[49] S. Iijima, others, Helical microtubules of graphitic carbon, Nature. 354 (1991) 56–58.

[50] Examples of the I.S.A.A.C.S. program, (n.d.). http://isaacs.sourceforge.net/ex.html (accessed October 2, 2015).

[51] Single-wall Carbon Nanotubes - Carbon Allotropes: Graphene, Nanotubes, Diamond & Fullerene Products, (n.d.). http://www.carbonallotropes.com/carbon-nanotubes/39-single-wall-carbon-nanotubes.html (accessed October 2, 2015).

[52] Y. Bin Tan, J.-M. Lee, Graphene for supercapacitor applications, J. Mater. Chem. A. 1 (2013) 14814–14843.

[53] K.S. Novoselov, A.K. Geim, S. V Morozov, D. Jiang, Y. Zhang, S. V Dubonos, et al., Electric field effect in atomically thin carbon films, Science (80-.). 306 (2004) 666–669.

[54] Logic gates in graphene technology | Solid State Technology, (n.d.). http://electroiq.com/blog/2013/09/logic-gates-in-graphene-technology/ (accessed October 2, 2015).

[55] D. V Kosynkin, A.L. Higginbotham, A. Sinitskii, J.R. Lomeda, A. Dimiev, B.K. Price, et al., Longitudinal unzipping of carbon nanotubes to form graphene nanoribbons, Nature. 458 (2009) 872–876.

[56] K.S. Subrahmanyam, L.S. Panchakarla, A. Govindaraj, C.N.R. Rao, Simple method of preparing graphene flakes by an arc-discharge method, J. Phys. Chem. C. 113 (2009) 4257–4259.

[57] W. Chen, L. Yan, P.R. Bangal, Preparation of graphene by the rapid and mild thermal reduction of graphene oxide induced by microwaves, Carbon N. Y. 48 (2010) 1146–1152.

[58] S. Stankovich, D.A. Dikin, R.D. Piner, K.A. Kohlhaas, A. Kleinhammes, Y. Jia, et al., Synthesis of graphene-based nanosheets via chemical reduction of exfoliated graphite oxide, Carbon N. Y. 45 (2007) 1558–1565.

[59] Y.L. Zhong, Z. Tian, G.P. Simon, D. Li, Scalable production of graphene via wet chemistry: progress and challenges, Mater. Today. (2014).

[60] R. Trusovas, K. Ratautas, G. Račiukaitis, J. Barkauskas, I. Stankevičien\.e, G. Niaura, et al., Reduction of graphite oxide to graphene with laser irradiation, Carbon N. Y. 52 (2013) 574–582.

[61] M. Inagaki, Y.A. Kim, M. Endo, Graphene: preparation and structural perfection, J. Mater. Chem. 21 (2011) 3280–3294.

[62] Q. Yu, J. Lian, S. Siriponglert, H. Li, Y.P. Chen, S.-S. Pei, Graphene segregated on Ni surfaces and transferred to insulators, Appl. Phys. Lett. 93 (2008) 113103. doi:10.1063/1.2982585.

[63] K.S. Kim, Y. Zhao, H. Jang, S.Y. Lee, J.M. Kim, K.S. Kim, et al., Large-scale pattern growth of graphene films for stretchable transparent electrodes, Nature. 457 (2009) 706–710.

[64] X. Li, W. Cai, J. An, S. Kim, J. Nah, D. Yang, et al., Large-area synthesis of high-quality and uniform graphene films on copper foils, Science (80-.). 324 (2009) 1312–1314.

[65] A. Reina, S. Thiele, X. Jia, S. Bhaviripudi, M.S. Dresselhaus, J.A. Schaefer, et al., Growth of large-area single-and bi-layer graphene by controlled carbon precipitation on polycrystalline Ni surfaces, Nano Res. 2 (2009) 509–516.

[66] L. Gao, W. Ren, H. Xu, L. Jin, Z. Wang, T. Ma, et al., Repeated growth and bubbling transfer of graphene with millimetre-size single-crystal grains using platinum., Nat. Commun. 3 (2012) 699. doi:10.1038/ncomms1702.

[67] H. Ago, Y. Ito, N. Mizuta, K. Yoshida, B. Hu, C.M. Orofeo, et al., Epitaxial chemical vapor deposition growth of single-layer graphene over cobalt film crystallized on sapphire., ACS Nano. 4 (2010) 7407–14. doi:10.1021/nn102519b.

[68] A.K. V Skákalová, Graphene: Properties, Preparation, Characterisation and Devices, Elsevier Science, 2014. https://books.google.com/books?hl=en&lr=&id=rf6iAgAAQBAJ&pgis=1 (accessed April 11, 2015).

[69] X. Cao, Y. Shi, W. Shi, G. Lu, X. Huang, Q. Yan, et al., Preparation of novel 3D graphene networks for supercapacitor applications, Small. 7 (2011) 3163–3168.

[70] A.K. Geim, K.S. Novoselov, The rise of graphene, Nat. Mater. 6 (2007) 183–191.

[71] T. Yu, E.-K. Lee, B. Briggs, B. Nagabhirava, B. Yu, Bilayer graphene system: current-induced reliability limit, Electron Device Lett. IEEE. 31 (2010) 1155–1157.

[72] K.-J. Lee, A.P. Chandrakasan, J. Kong, Breakdown current density of CVD-grown multilayer graphene interconnects, Electron Device Lett. IEEE. 32 (2011) 557–559.

[73] R. Murali, Y. Yang, K. Brenner, T. Beck, J.D. Meindl, Breakdown current density of graphene nanoribbons, Appl. Phys. Lett. 94 (2009) 243114.

[74] M.C. Wang, C. Yan, L. Ma, N. Hu, M.W. Chen, Effect of defects on fracture strength of graphene sheets, Comput. Mater. Sci. 54 (2012) 236–239.

[75] K.S. Novoselov, A.K. Geim, S. V Morozov, D. Jiang, M.I. Katsnelson, I. V Grigorieva, et al., Two-dimensional gas of massless Dirac fermions in graphene., Nature. 438 (2005) 197–200. doi:10.1038/nature04233.

[76] N.M.R. Peres, A.H. Castro Neto, F. Guinea, Dirac fermion confinement in graphene,

Phys. Rev. B. 73 (2006) 241403. doi:10.1103/PhysRevB.73.241403.

[77] N.F. Atta, Nanosensors: Materials and Technologies, Lulu.com, 2013. https://books.google.com/books?id=e5LFBgAAQBAJ&pgis=1 (accessed April 11, 2015).

[78] M. Endo, T. Maeda, T. Takeda, Y.J. Kim, K. Koshiba, H. Hara, et al., Capacitance and Pore-Size Distribution in Aqueous and Nonaqueous Electrolytes Using Various Activated Carbon Electrodes, J. Electrochem. Soc. 148 (2001) A910. doi:10.1149/1.1382589.

[79] S. Shiraishi, H. Kurihara, K. Okabe, D. Hulicova, A. Oya, Electric double layer capacitance of highly pure single-walled carbon nanotubes (HiPco^{TM}Buckytubes^{TM}) in propylene carbonate electrolytes, Electrochem. Commun. 4 (2002) 593–598. doi:10.1016/S1388-2481(02)00382-X.

[80] J. Lee, J. Kim, T. Hyeon, Recent Progress in the Synthesis of Porous Carbon Materials, Adv. Mater. 18 (2006) 2073–2094. doi:10.1002/adma.200501576.

[81] C. Liu, Z. Yu, D. Neff, A. Zhamu, B.Z. Jang, Graphene-based supercapacitor with an ultrahigh energy density., Nano Lett. 10 (2010) 4863–8. doi:10.1021/nl102661q.

[82] Y. Wang, Z. Shi, Y. Huang, Y. Ma, C. Wang, M. Chen, et al., Supercapacitor devices based on graphene materials, J. Phys. Chem. C. 113 (2009) 13103–13107.

[83] F. Regisser, M.-A. Lavoie, G.Y. Champagne, D. Bélanger, Randomly oriented graphite electrode. Part 1. Effect of electrochemical pretreatment on the electrochemical behavior and chemical composition of the electrode, J. Electroanal. Chem. 415 (1996) 47–54. doi:10.1016/S0022-0728(96)04636-0.

[84] F. Béguin, K. Szostak, G. Lota, E. Frackowiak, A Self-Supporting Electrode for Supercapacitors Prepared by One-Step Pyrolysis of Carbon Nanotube/Polyacrylonitrile Blends, Adv. Mater. 17 (2005) 2380–2384.

[85] K. Leitner, A. Lerf, M. Winter, J.O. Besenhard, S. Villar-Rodil, F. Suárez-García, et al., Nomex-derived activated carbon fibers as electrode materials in carbon based supercapacitors, J. Power Sources. 153 (2006) 419–423. doi:10.1016/j.jpowsour.2005.05.078.

[86] E. Frackowiak, F. Béguin, Carbon materials for the electrochemical storage of energy in capacitors, Carbon N. Y. 39 (2001) 937–950. doi:10.1016/S0008-6223(00)00183-4.

[87] H. Wang, H.S. Casalongue, Y. Liang, H. Dai, Ni(OH)2 nanoplates grown on graphene as advanced electrochemical pseudocapacitor materials., J. Am. Chem. Soc. 132 (2010) 7472–7. doi:10.1021/ja102267j.

[88] Z.-S. Wu, D.-W. Wang, W. Ren, J. Zhao, G. Zhou, F. Li, et al., Anchoring Hydrous RuO2 on Graphene Sheets for High-Performance Electrochemical Capacitors, Adv. Funct.

Mater. 20 (2010) 3595–3602. doi:10.1002/adfm.201001054.

[89] L.L. Zhang, T. Wei, W. Wang, X.S. Zhao, Manganese oxide–carbon composite as supercapacitor electrode materials, Microporous Mesoporous Mater. 123 (2009) 260–267. doi:10.1016/j.micromeso.2009.04.008.

[90] Z.-S. Wu, G. Zhou, L.-C. Yin, W. Ren, F. Li, H.-M. Cheng, Graphene/metal oxide composite electrode materials for energy storage, Nano Energy. 1 (2012) 107–131. doi:10.1016/j.nanoen.2011.11.001.

[91] X. Dong, L. Wang, D. Wang, C. Li, J. Jin, Layer-by-Layer Engineered Co À Al Hydroxide Nanosheets / Graphene Multilayer Films as Flexible Electrode for Supercapacitor, (2011) 2–7.

[92] L.L. Zhang, S. Zhao, X.N. Tian, X.S. Zhao, Layered graphene oxide nanostructures with sandwiched conducting polymers as supercapacitor electrodes., Langmuir. 26 (2010) 17624–8. doi:10.1021/la103413s.

[93] S. Trasatti, G. Buzzanca, Ruthenium dioxide: a new interesting electrode material. Solid state structure and electrochemical behaviour, J. Electroanal. Chem. Interfacial Electrochem. 29 (1971) A1–A5.

[94] E. Herrero, L.J. Buller, H.D. Abruna, Underpotential deposition at single crystal surfaces of Au, Pt, Ag and other materials, Chem. Rev. 101 (2001) 1897–1930.

[95] J.P. Zheng, P.J. Cygan, T.R. Jow, Hydrous ruthenium oxide as an electrode material for electrochemical capacitors, J. Electrochem. Soc. 142 (1995) 2699–2703.

[96] T. Brousse, M. Toupin, R. Dugas, L. Athouël, O. Crosnier, D. Bélanger, Crystalline MnO2 as possible alternatives to amorphous compounds in electrochemical supercapacitors, J. Electrochem. Soc. 153 (2006) A2171–A2180.

[97] D.-W. Wang, F. Li, H.-M. Cheng, Hierarchical porous nickel oxide and carbon as electrode materials for asymmetric supercapacitor, J. Power Sources. 185 (2008) 1563–1568.

[98] V. Augustyn, J. Come, M.A. Lowe, J.W. Kim, P.-L. Taberna, S.H. Tolbert, et al., High-rate electrochemical energy storage through Li+ intercalation pseudocapacitance, Nat. Mater. 12 (2013) 518–522.

[99] M. Okubo, E. Hosono, J. Kim, M. Enomoto, N. Kojima, T. Kudo, et al., Nanosize effect on high-rate Li-ion intercalation in LiCoO2 electrode, J. Am. Chem. Soc. 129 (2007) 7444–7452.

[100] E. Manasse, Idrotalcite e piroaurite, Stab. tipografico succ. FF. Nistri, 1915.

[101] X. Duan, D.G. Evans, Layered double hydroxides, Springer Science & Business Media, 2006.

[102] D. Tichit, A. Rolland, F. Prinetto, G. Fetter, M. de Jesus Martinez-Ortiz, M. a. Valenzuela, et al., Comparison of the structural and acid-base properties of Ga- and Al-containing layered double hydroxides obtained by microwave irradiation and conventional ageing of synthesis gels, J. Mater. Chem. 12 (2002) 3832–3838. doi:10.1039/b203376n.

[103] H. Abdolmohammad-Zadeh, S. Kohansal, Determination of mesalamine by spectrofluorometry in human serum after solid-phase extraction with Ni-Al layered double hydroxide as a nanosorbent, J. Braz. Chem. Soc. 23 (2012) 473–481.

[104] A. Malak-Polaczyk, C. Vix-Guterl, E. Frackowiak, Carbon/layered double hydroxide (LDH) composites for supercapacitor application, Energy and Fuels. 24 (2010) 3346–3351. doi:10.1021/ef901505c.

[105] C. Mousty, V. Prévot, Hybrid and biohybrid layered double hydroxides for electrochemical analysis, Anal. Bioanal. Chem. 405 (2013) 3513–3523.

[106] V. Rives, Layered double hydroxides: present and future, Nova Publishers, 2001.

[107] C. Mousty, V. Prévot, Hybrid and biohybrid layered double hydroxides for electrochemical analysis, Anal. Bioanal. Chem. 405 (2013) 3513–3523. doi:10.1007/s00216-013-6797-1.

[108] M. Sipiczki, Functional Materials- Syntheses, Characterisation and Catalytic Applications, (2013).

[109] R. Ma, T. Sasaki, Synthesis of LDH nanosheets and their layer-by-layer assembly, Recent Pat. Nanotechnol. 6 (2012) 159–168.

[110] F.L. Theiss, Synthesis and characterisation of layered double hydroxides and their application for water purification, (2012).

[111] S. Nishimura, A. Takagaki, K. Ebitani, Characterization, synthesis and catalysis of hydrotalcite-related materials for highly efficient materials transformations, Green Chem. 15 (2013) 2026–2042. doi:10.1039/C3GC40405F.

[112] J. Olanrewaju, B.L. Newalkar, C. Mancino, S. Komarneni, Simplified synthesis of nitrate form of layered double hydroxide, Mater. Lett. 45 (2000) 307–310.

[113] S. Miyata, Hydrotalcites in relation to composition, Clays Clay Min. 28 (1980) 50–56.

[114] F. Cavani, F. Trifirò, A. Vaccari, Hydrotalcite-type anionic clays: Preparation, properties and applications., Catal. Today. 11 (1991) 173–301.

[115] B. Sels, D. De Vos, M. Buntinx, F. Pierard, a Kirsch-De Mesmaeker, P. Jacobs, Layered

double hydroxides exchanged with tungstate as biomimetic catalysts for mild oxidative bromination, Nature. 400 (1999) 855–857. doi:10.1038/23674.

[116] B.F. Sels, D.E. De Vos, P. a Jacobs, Hydrotalcite-like anionic clays in catalytic organic reactions, Catal Rev Sci Eng F. Full J. TitleCatalysis Rev. Sci. Eng. 43 (2001) 443–488. doi:10.1081/CR-120001809.

[117] T.-Y. Wei, C.-H. Chen, K.-H. Chang, S.-Y. Lu, C.-C. Hu, Cobalt oxide aerogels of ideal supercapacitive properties prepared with an epoxide synthetic route, Chem. Mater. 21 (2009) 3228–3233.

[118] H. Chen, F. Zhang, S. Fu, X. Duan, In situ microstructure control of oriented layered double hydroxide monolayer films with curved hexagonal crystals as superhydrophobic materials, Adv. Mater. 18 (2006) 3089–3093. doi:10.1002/adma.200600615.

[119] H. Chen, L. Hu, M. Chen, Y. Yan, L. Wu, Nickel-Cobalt Layered Double Hydroxide Nanosheets for High-performance Supercapacitor Electrode Materials, Adv. Funct. Mater. 24 (2014) 934–942. doi:10.1002/adfm.201301747.

[120] Y. Song, J. Wang, Z. Li, D. Guan, T. Mann, Q. Liu, et al., Self-assembled hierarchical porous layered double hydroxides by solvothermal method and their application for capacitors, Microporous Mesoporous Mater. 148 (2012) 159–165. doi:10.1016/j.micromeso.2011.08.013.

[121] Z. Wang, X. Zhang, J. Wang, L. Zou, Z. Liu, Z. Hao, Preparation and capacitance properties of graphene/NiAl layered double-hydroxide nanocomposite., J. Colloid Interface Sci. 396 (2013) 251–7. doi:10.1016/j.jcis.2013.01.013.

[122] W. Zhang, C. Ma, J. Fang, J. Cheng, X. Zhang, S. Dong, et al., Asymmetric electrochemical capacitors with high energy and power density based on graphene/CoAl-LDH and activated carbon electrodes, RSC Adv. 3 (2013) 2483. doi:10.1039/c2ra23283a.

[123] L. Wang, D. Wang, X.Y. Dong, Z.J. Zhang, X.F. Pei, X.J. Chen, et al., Layered assembly of graphene oxide and Co-Al layered double hydroxide nanosheets as electrode materials for supercapacitors., Chem. Commun. (Camb). 47 (2011) 3556–3558. doi:10.1039/c0cc05420h.

[124] N. Yulian, L. Ruiyi, L. Zaijun, F. Yinjun, L. Junkang, High-performance supercapacitors materials prepared via in situ growth of NiAl-layered double hydroxide nanoflakes on well-activated graphene nanosheets, Electrochim. Acta. 94 (2013) 360–366. doi:10.1016/j.electacta.2012.09.084.

[125] W. Yang, Z. Gao, J. Wang, J. Ma, M. Zhang, L. Liu, Solvothermal one-step synthesis of Ni-Al layered double hydroxide/carbon nanotube/reduced graphene oxide sheet ternary nanocomposite with ultrahigh capacitance for supercapacitors., ACS Appl. Mater.

Interfaces. 5 (2013) 5443–54. doi:10.1021/am4003843.

[126] B. Wang, Q. Liu, Z. Qian, X. Zhang, J. Wang, Z. Li, et al., Two steps in situ structure fabrication of Ni-Al layered double hydroxide on Ni foam and its electrochemical performance for supercapacitors, J. Power Sources. 246 (2014) 747–753. doi:10.1016/j.jpowsour.2013.08.035.

[127] Y. Zhang, L. Zhang, C. Zhou, Review of chemical vapor deposition of graphene and related applications., Acc. Chem. Res. 46 (2013) 2329–39. doi:10.1021/ar300203n.

[128] B. Abdulhakeem, Three dimensional graphene composites for energy storage applications, University of Pretoria, 2014.

[129] B.L. Hayes, others, Recent advances in microwave-assisted synthesis, Aldrichimica Acta. 37 (2004) 66–77.

[130] B.I. Kharisov, O. V Kharissova, U.O. Méndez, Microwave hydrothermal and solvothermal processing of materials and compounds, INTECH Open Access Publisher, 2012.

[131] www.sustainablechemicalprocesses.com - Figure, (n.d.). http://www.sustainablechemicalprocesses.com/content/1/1/5/figure/F1 (accessed October 2, 2015).

[132] I. Bilecka, M. Niederberger, Microwave chemistry for inorganic nanomaterials synthesis, Nanoscale. 2 (2010) 1358–1374.

[133] D.M.P. Mingos, D.R. Baghurst, Tilden Lecture. Applications of microwave dielectric heating effects to synthetic problems in chemistry, Chem. Soc. Rev. 20 (1991) 1–47.

[134] A. Loupy, Microwaves in organic synthesis, Wiley-VCH; John Wiley, distributor], 2006.

[135] C.O. Kappe, A. Stadler, D. Dallinger, Microwaves in organic and medicinal chemistry, John Wiley & Sons, 2012.

[136] C.O. Kappe, Microwave dielectric heating in synthetic organic chemistry, Chem. Soc. Rev. 37 (2008) 1127–1139.

[137] A. Sciences, Three dimensional graphene composites for energy storage applications by Bello Abdulhakeem A thesis submitted in partial fulfilment of the requirements for the degree of DOCTOR OF PHILOSOPHY (PHD) IN PHYSICS Faculty of Natural and Agricultural Sciences , (2014).

[138] C.O. Kappe, D. Dallinger, Controlled microwave heating in modern organic synthesis: highlights from the 2004--2008 literature, Mol. Divers. 13 (2009) 71–193.

[139] Y. Li, J. Wang, Y. Zhang, M.N. Banis, J. Liu, D. Geng, et al., Facile controlled synthesis

and growth mechanisms of flower-like and tubular MnO 2 nanostructures by microwave-assisted hydrothermal method, J. Colloid Interface Sci. 369 (2012) 123–128.

[140] Y. Leng, Materials characterization: introduction to microscopic and spectroscopic methods, John Wiley & Sons, 2009.

[141] J. Goldstein, D.E. Newbury, P. Echlin, D.C. Joy, A.D. Romig Jr, C.E. Lyman, et al., Scanning electron microscopy and X-ray microanalysis: a text for biologists, materials scientists, and geologists, Springer Science & Business Media, 2012.

[142] B.D. Cullity, S.R. Stock, Elements of X-ray Diffraction, Prentice hall Upper Saddle River, NJ, 2001.

[143] Charl Jeremy Jafta, Synthetic strategies to improve the performance of manganese oxide based layered and spinel materials for electrochemical energy storage, University of Pretoria, 2014.

[144] D. Gardiner, P. Graves, H. Bowley, Practical Raman Spectroscopy, Springer-Verlag Berlin Heidelberg, 1989.

[145] N.K. Nayyar, G.S. Murty, The stability of a dielectric liquid jet in the presence of a longitudinal electric field, Proc. Phys. Soc. 75 (1960) 369.

[146] F. Barzegar, Synthesis and characterization of Polymer/Graphene electrospun nanofibers, (2014).

[147] A. Ferrari, Raman spectroscopy of graphene and graphite: disorder, electron–phonon coupling, doping and nonadiabatic effects, Solid State Commun. 143 (2007) 47–57. doi:10.1016/j.ssc.2007.03.052.

[148] A. Jorio, C.A. Achete, E.H.M. Ferreira, L.G. Cançado, R.B. Capaz, Measuring disorder in graphene with Raman spectroscopy, INTECH Open Access Publisher, 2011.

[149] M.A. Pimenta, G. Dresselhaus, M.S. Dresselhaus, L.G. Cançado, A. Jorio, R. Saito, Studying disorder in graphite-based systems by Raman spectroscopy., Phys. Chem. Chem. Phys. 9 (2007) 1276–1291. doi:10.1039/b613962k.

[150] M.D. Yusuf, Investigation of metal hydroxides-graphene composites as electrode materials for supercapacitor applications, University of Pretoria, 2015.

[151] W. Yang, Z. Gao, J. Wang, J. Ma, M. Zhang, L. Liu, Solvothermal one-step synthesis of Ni-Al layered double hydroxide/carbon nanotube/reduced graphene oxide sheet ternary nanocomposite with ultrahigh capacitance for supercapacitors., ACS Appl. Mater. Interfaces. 5 (2013) 5443–5454.

[152] W. Zhang, C. Ma, J. Fang, J. Cheng, X. Zhang, S. Dong, et al., Asymmetric

electrochemical capacitors with high energy and power density based on graphene/CoAl-LDH and activated carbon electrodes, RSC Adv. 3 (2013) 2483–2490.

[153] Y.-S. Bae, A.O. Yazayd\in, R.Q. Snurr, Evaluation of the BET method for determining surface areas of MOFs and zeolites that contain ultra-micropores, Langmuir. 26 (2010) 5475–5483.

[154] D. Dobos, Electrochemical data: a handbook for electrochemists in industry and universities, Elsevier Science & Technology, 1975.

[155] N. Hong, L. Song, B. Wang, A.A. Stec, T.R. Hull, J. Zhan, et al., Co-precipitation synthesis of reduced graphene oxide/NiAl-layered double hydroxide hybrid and its application in flame retarding poly (methyl methacrylate), Mater. Res. Bull. 49 (2014) 657–664.

[156] Z.-A. Hu, Y.-L. Xie, Y.-X. Wang, H.-Y. Wu, Y.-Y. Yang, Z.-Y. Zhang, Synthesis and electrochemical characterization of mesoporous CoxNi1−x layered double hydroxides as electrode materials for supercapacitors, Electrochim. Acta. 54 (2009) 2737–2741. doi:10.1016/j.electacta.2008.11.035.

[157] C. Weidenthaler, Pitfalls in the characterization of nanoporous and nanosized materials, Nanoscale. 3 (2011) 792–810.

[158] W.-H. Zhu, J.-J. Ke, H.-M. Yu, D.-J. Zhang, A study of the electrochemistry of nickel hydroxide electrodes with various additives, J. Power Sources. 56 (1995) 75–79. doi:10.1016/0378-7753(95)80011-5.

[159] F. Barzegar, A. Bello, O.O. Fashedemi, J.K. Dangbegnon, D.Y. Momodu, F. Taghizadeh, et al., Synthesis of 3D porous carbon based on cheap polymers and graphene foam for high-performance electrochemical capacitors, Electrochim. Acta. 180 (2015) 442–450. doi:10.1016/j.electacta.2015.08.148.